Final Report

Contract Number: DTPH56-14-H-CAP01

Prepared for: DOT

Project Title: Patch and Full-Encirclement Repairs for Through-Wall Defects

Prepared By: The University of Tulsa

Contact Information: Michael W. Keller, mwkeller@utulsa.edu, 918-631-3198

Executive Summary

The objective of the research presented in this report was to investigate the performance of patch-type composite repairs on pressure vessels with through-wall defects. The most common repair geometry for bonded composites is the full-encirclement repair where the repair is formed by installing a composite that completely encircles the damaged substrate. These repairs are straightforward to install and have proven to have good field performance through a variety of industry and academic-sponsored research projects. When the substrate vessel becomes large, then these encirclement repairs begin to become cumbersome and costly to install. A potential alternative is to use, instead, an adhesively bonded patch that does not encircle the substrate. Patch-type repairs have been used for almost two decades in the aerospace industry, but are not a common or accepted repair type for pressure vessels. The primary goal of the research in the present study was to understand the differences between full-encirclement and patch repairs on through-wall defects.

This study consisted of an experimental investigation of the fatigue performance of patch repairs and a computational study of the same geometry. For the experimental study, a 0.50 in through-wall defect was machined into straight sections of 6-inch ASTM 106B pipe. A follow-on study used a 42 in OD test vessel with identical 0.5 in through-wall defects. Fatigue testing consisted of pressurizing these samples from 0 to 500 psi until failure or runout of 100,000 cycles was reached. A total of 18 small scale specimens were tested, 9 patch repairs and 9 full-encirclement repairs. With three different industry participants

installing repairs on these samples. Substrate and composite strains were measured using installed strain gages and via digital image correlation (DIC). The DIC measurements provided a full-field measurement of strain during a pressure cycle.

Average fatigue life for full-encirclement repairs was 31,352 cycles with a standard deviation of 42,768 cycles. Patch repairs exhibited an average fatigue life of 39,896 cycles with a standard deviation of 38,239 cycles. Two patch repairs and two full-encirclement repairs reached runout of 100,000 cycles. Strain levels in all composite repairs tended to increase as fatigue cycles increased. Strain gage and DIC measurements show that for all specimens except two, strains are higher in full-encirclement repairs than in patch repairs. After the small-scale tests were completed, a large scale vessel test was initiated. Patch repairs of the same design were installed on at 42 inch vessel and cycled from 80 psi to 500 psi, which matched the pressure range on the small scale specimens. Current results indicate that the repairs on the small-scale specimens behave similarly to tests on the large scale specimens. Based on fatigue and strain data presented in this report, patch repairs are likely appropriate for through-wall defects and can be expected to perform similarly to full-encirclement repairs.

Contents

Chapter 1

INTRODUCTION

1.1 Background

Pipelines are among the safest and most efficient methods of transporting oil and natural gas across long distances [1]. Over 1.7 million kilometers of oil transmission pipelines exist worldwide and over 60% of these pipelines have been in service for over 40 years[2, 3]. Many of these pipelines are subjected to external corrosive environments, such as salt water, sulphur ingress media, or groundwater, which can cause stress corrosion cracking and wall loss [1, 4]. The United States alone spends approximately $7 billion annually on repairing pipeline corrosion damage in the oil and gas industry [5]. Traditionally, sections of steel pipelines with corrosion damage are either removed and completely replaced or reinforced with a two-part steel sleeve. These traditional repairs can be expensive, dangerous, and difficult to install in underground piping systems as well as close-spaced pipe racks in plants [6]. The difficulties associated with traditional repairs encouraged the research and devel-

opment of fiber-reinforced polymeric composite (FRPC) over-wraps in the early 1990's. Since then, many studies have investigated the use of FRPC's in pipelines [7, 8, 9]

Composite repairs have gained increased acceptance in several industries including infrastructure, aerospace, automotive, and oil & gas [10]. This acceptance can be attributed to several inherent advantages that FRPC's possess, including superior strength-to-weight ratios, toughness, moisture & chemical resistance, and formability to complex geometries [11]. These factors have caused the recent use of FRPC over-wraps in pipeline repair systems by oil & gas companies.

In addition to mechanical advantages, FRPC's also offer several economic advantages over traditional steel repairs. In fact, in an industry study, FRPC repairs were shown to be more economically viable as early as 1995 for some cases [12]. The major contributing factor considered in these calculations was the ability for FRPC repairs to be installed while the pipeline is online, or live [13]. Live repairs are not an option for traditional steel repairs due to the potential for section removal or hot-working. Complete shutdown of a pipeline is costly and ultimately results in higher energy costs for consumers.

1.1.1 Pipeline Over-Wrap Repairs

FRPC repairs consist of a woven fabric with continuous fiber reinforcement coupled with a thermoset polymeric matrix. The damaged section of pipe is prepared by thoroughly cleaning the surface with sanding or grit blasting and then applying a primer. Lastly, the repair is completed by wrapping the wetted out fabric around the pipe and leaving at room temperature to cure.

Traditionally, repairs completely encircle the pipe as shown below in Figure 1.1a. This

type of repair is referred to as a full-encirclement repair and is accepted as the industry standard for composite repairs. However, as familiarity with composite repairs increased in the oil & gas industry, engineers and technicians began to consider larger pipelines and pressure vessels as potential sites for composite repair application. These larger pipelines can be significantly more expensive to repair due to an increase in material and labor cost. Additionally, larger full-encirclement installations can be cumbersome to wrap completely around damaged pressure equipment. Therefore, patch-type repair systems have been considered as a viable alternative. Patch repairs, shown below in Figure 1.1b, differ from full-encirclement repairs in that they do not wrap the composite completely around the damaged section of pipe, but rather over only a specified section, or patch, of the pipe. These patch type repairs have been used in the aerospace industry for over a decade ,but have yet to become widely accepted in the oil & gas industry due to the lack of relevant performance data.

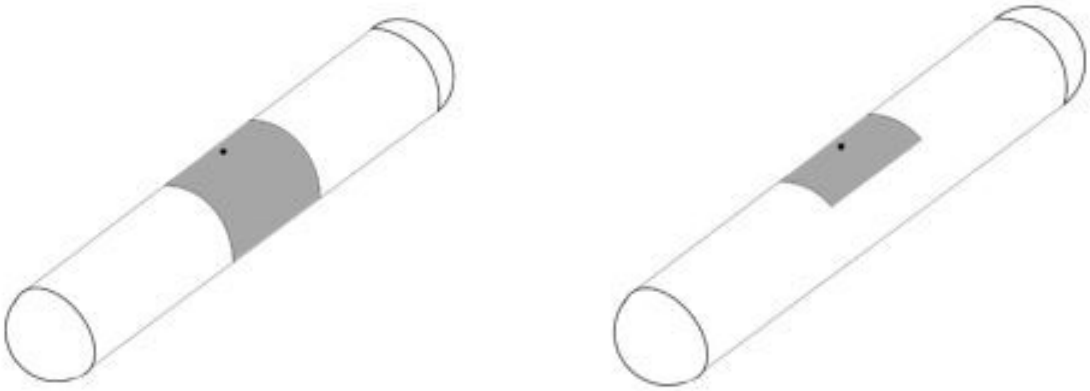

(a) Full encirclement repair (b) Patch-type repair

Figure 1.1: Repair material preparation

1.1.2 Federal Regulations

Currently, Department of Transportation (DOT) regulations stipulate the procedure for repair of any defect that reduces the wall thickness below that required by maximum allowable operating pressure (MAOP) in a gas transmission pipeline. The segment of pipe that contains these defects must be either replaced or "the operating pressure reduced commensurate with the strength of the pipe based on actual remaining wall thickness". Alternatively, regulations also allow for repairs that "reliable engineering tests and analyses show can permanently restore the serviceability of the pipe" [14]. A similar regulation exists for sections of corroded pipelines carrying other potentially hazardous liquids [15].

ASME PCC-2 and ISO 24817 standards stipulate full-encirclement repair dimensions such as length of the repair from the defect and repair thickness [16, 17]. Currently, standards offer guidelines for patch-type repairs, but these guidelines are untested.

1.2 Research Objectives

The primary goal of this research is to determine the viability of patch type repairs in 6-inch diameter pipelines with through-wall defects. Through-wall defects, also referred to as leaking defects, are defined as flaws that have completely penetrated the wall of the pipeline or that will grow through the wall during the lifetime of the installed repair. Alternatively, non-leaking defects are flaws that have not completely penetrated the wall of the pipeline, but only damaged a portion of the wall thickness. The specific goals of the research presented in this report are to generate a reliable finite element model that properly describes the anisotropic behavior of the FRPC repair, to characterize the strain response of both full-encirclement and patch type repairs in small scale testing of 6-inch diameter ASTM 106b steel pipes, to determine if patch type repairs are a viable alternative to full-encirclement repairs in small scale testing, and lastly to quantitatively compare data acquired via strain gages to data acquired via digital image correlation (DIC).

Chapter 2

Composite Repair System Description

The repair system can consist of four distinct materials: the reinforcing fabric, a thermosetting matrix, a primer, and a dimensional restoration putty. In the case of through-wall defects, the dimensional restoration putty is not needed.

2.1 Reinforcing Fabric

The fiber reinforced fabrics used in this study had a plain-weave architecture. A schematic of this weave is shown below in Figure 2.1. Warp threads and filling threads are oriented 90° from each other and interlaced in an alternating pattern.

The number of fibers in each individual bundle, referred to as the tow count, is determined by a number of factors. Typically, pipe geometry and defect size are the most important design criteria when considering a composite repair. For example, a pipe elbow may be large and require a large repair, but the reinforcing fabric must still be pliable enough to conform to the pipe. It should be noted that the tow count in the warp and

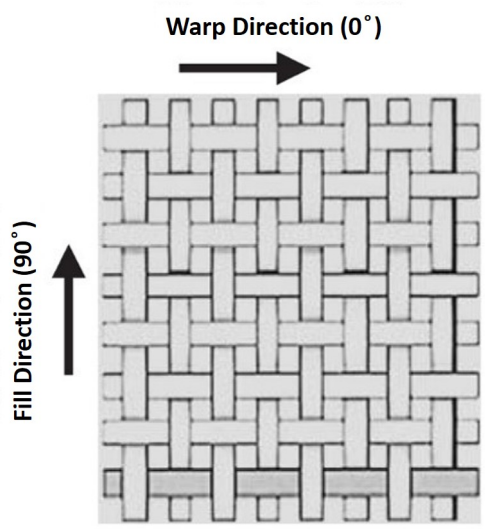

Figure 2.1: Schematic of Plain Weave Architecture [18]

fill directions is often different, implying that one direction of the fabric is stiffer than the other.

2.2 Thermoset Matrerial and Primer

Each company that repaired pipes in this study used their own proprietary thermosetting material. Two of the three companies that installed repairs used an epoxy matrix while the third company used a polyurethane matrix. However, each matrix consisted of two parts: a hardener and a resin. These two parts combined with the reinforcing fabric to form a monolithic structure. Each company also used their own two-part primer to help ensure bonding between the FRPC repair and the steel substrate.

2.3 Application Process

If a dimensional restoration putty is not being used in the repair process, the first step is to combine and thoroughly mix the two parts of the polymer matrix. The recently mixed epoxy is then applied to the fabric and evenly spread using a roller. These two processes are shown below in Figure 2.2.

(a) Mixing the epoxy matrix (b) Rolling the saturated fabric

Figure 2.2: Repair material preparation [19]

Next, the primer is mixed together and applied evenly to the damaged section of pipe, usually with a brush. The results of this process can be seen below in Figure 2.3 [19].

The saturated fabric can then be applied directly to the damaged section of the pipe. This is done by wrapping the fabric completely around the pipe while maintaining tension on the fabric to minimize the number of voids created by air bubbles during installation. Figure 2.4 shows the wrapping process and the final repair [19].

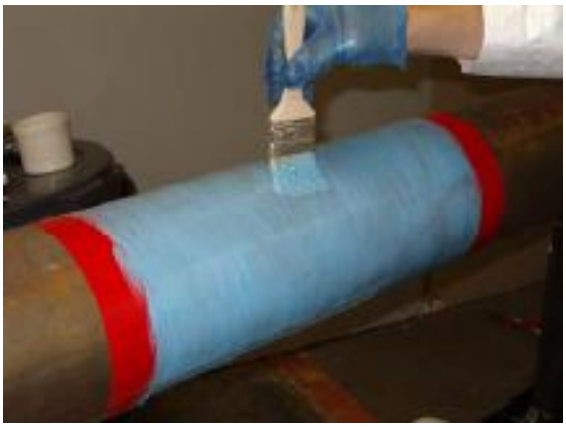

Figure 2.3: Application of primer

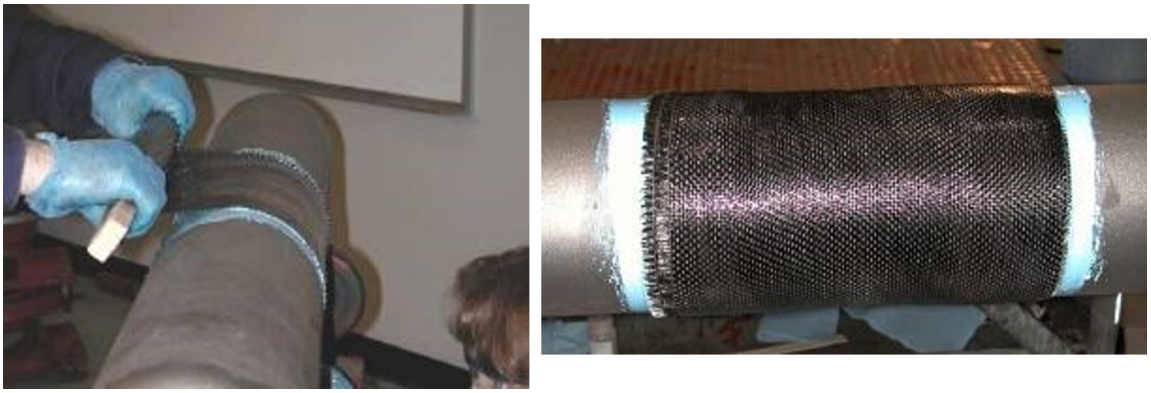

Figure 2.4: Wrapping of wetted out fabric (left) and final repair (right)

Chapter 3

Analytical and Computational Studies

This chapter describes the methods and results of computational finite element analysis and plate theory comparisons of patch and full-encirclement repairs. Each of these models consisted of a steel pipe substrate and a composite repair that required detailed modeling to ensure accurate results. These results provide overall trends that may be applicable to each of these repair types. Mesh convergence, L_{over}, and pressure load cycle simulations will be discussed in this chapter as well as a plate theory displacement comparison.

3.1 Material Model & Simulation Metrics

The simulated specimens were 4 foot long sections of 6-inch schedule 40 ASTM 106B pipe with a 0.50 in through-wall circular defect in the side as shown in figure B.1 in the Appendix. Specimens were modeled as quarter pipe sections with two symmetry boundary conditions as shown in Figure 3.1. These boundary conditions allowed for reduced computational time and increased mesh refinement in areas of interest during the simulation.

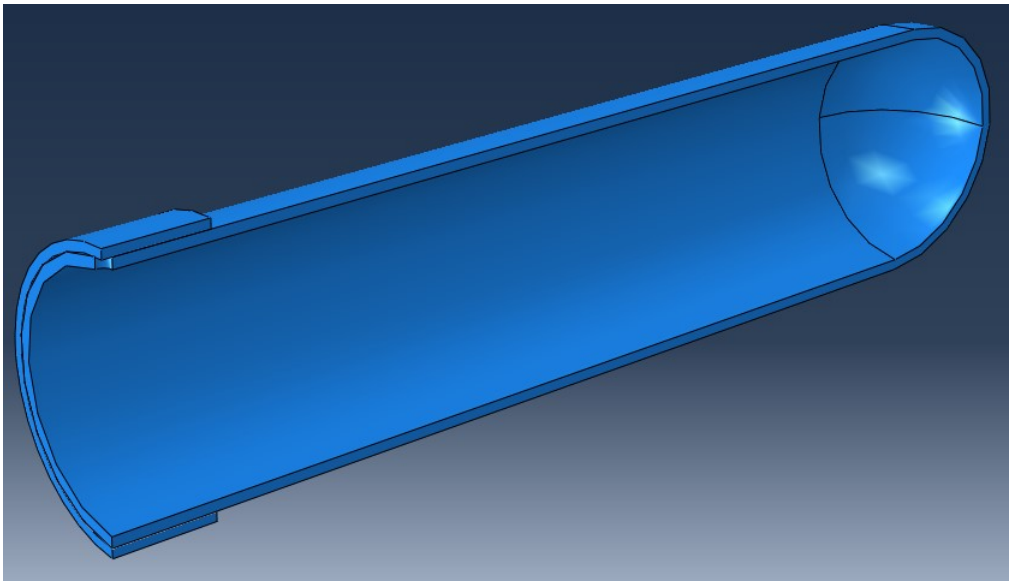

Figure 3.1: Small scale FEA modeled with symmetry boundary conditions

The composite overwrap was assumed to be perfectly bonded to the substrate and given appropriate anisotropic material properties obtained from testing [19]. The thickness of this repair was chosen to be 0.25 inch in order to appropriately represent realistic repair installations. Actual installed repair thickness will differ from the 0.25 in thickness used in the model, thus direct strain comparisons between strain gage measurements and the FEA model are not possible. Additionally, the total axial length of the repair was 5.55 in as required by ASME PCC-2 [17] for the given loading and geometry.

Substrate material properties for the ASTM 106B were obtained using quasi-static coupon testing from representative pipe sections that had been performed previously. Using this data, an elasto-plastic hardening model was constructed [20]. Material properties for both the substrate and composite repairs are shown in Figures A.1 and A.2.

3.2 Mesh Convergence

A mesh convergence study was conducted to determine the minimum global and local seed sizing in order to decrease overall computational time without sacrificing accuracy. In order to determine an appropriate local seed size, global seed sizes for the entire model were reduced at fixed increments and the resulting Von Mises stress were extracted. This method continued until the percent difference between maximum stresses in consecutive models was acceptably small. Next, areas of interest remained at the converged seed size while global seed size in the remainder of the geometry increased. Figure 3.2 below shows the results of the mesh convergence study for a hexagonal mesh.

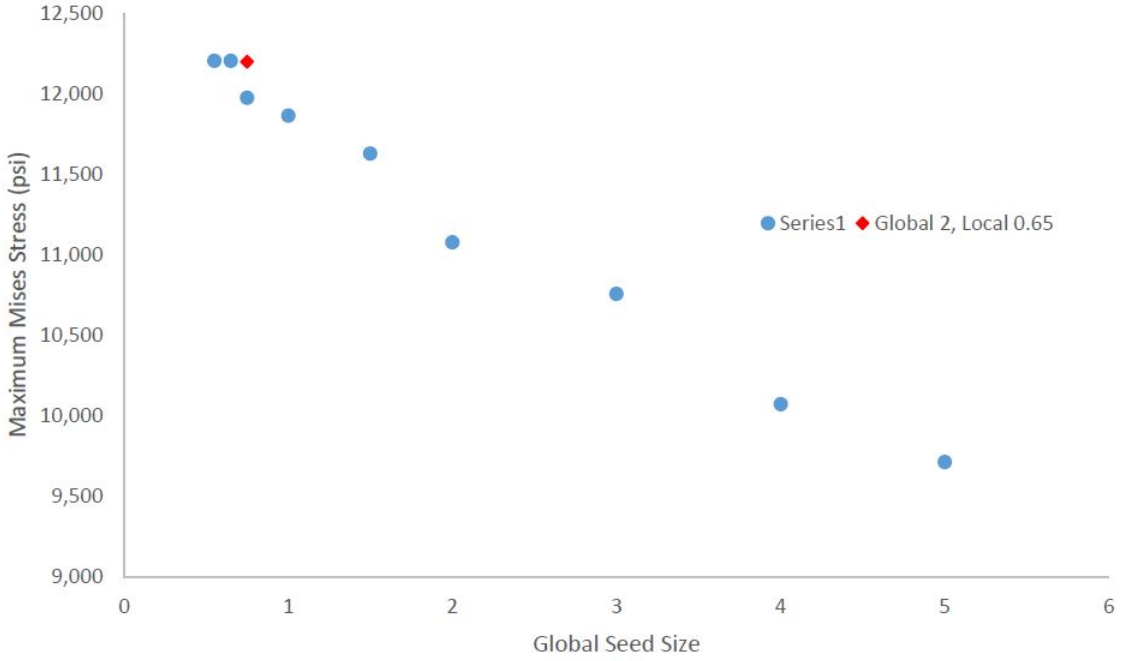

Figure 3.2: Comparison of strictly global seeds and combined seeding

As shown in 3.2, the maximum von Mises stress remained constant below a global seed

size of 0.65. Results of the study also show good agreement between models with an overall global seed size of 0.65 and combined global and local seed sizes of 2.0 and 0.65, respectively. Figure 3.3 below shows the refined mesh above the defect and the progressively coarser mesh in the steel substrate as the distance from the area of interest increases.

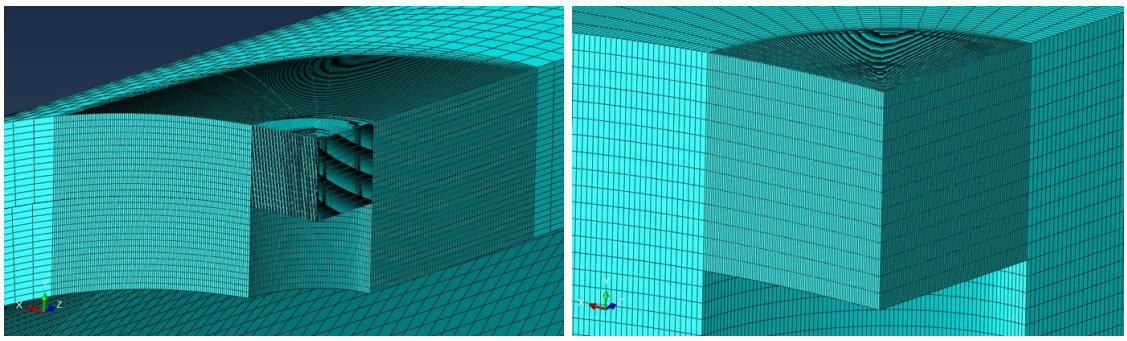

(a) Overall mesh convergence (b) Refinement over defect

Figure 3.3: Summary of mesh convergence study

3.3 Extent of Repair

The minimum distance that a repair must extend axially beyond the edge of the defect, referred to as L_{over}, is another primary design parameter for composite repairs. Depending on which material properties are known, ASME PCC-2 offers two different equations for calculating L_{over} shown in equations 3.1 and 3.2. If enough information is available to calculate both equations, the larger of the two L_{over} values is used.

$$L_{over} = 2.5\sqrt{Dt/2} \tag{3.1}$$

$$L_{over} = \frac{E_a \varepsilon_a t_{repair}}{\tau} \tag{3.2}$$

L_{over} = minimum distance repair full thickness of the repair that must extend past damaged region. This is considered the axial and circumferential distance for patch repairs.

D = external pipe diameter

t = nominal wall thickness of the substrate

E_a = tensile modulus of composite repair in the axial direction

ϵ_a = allowable axial strain of the composite

t_{repair} = design thickness of the composite repair

τ = lap shear strength of the composite

L_{over} was calculated to be 5.55 in for all specimens via equation 3.2 using the values below in Table 3.1. Values of L_{over} varied for each company due to variations in material properties.

Table 3.1: Material properties used in example L_{over} calculation

Metric	Value
E_a	3.17 Msi
e_a	0.013
t_{repair}	0.135 in
τ	1,000 psi

This value of L_{over} yielded a total repair length of 11.6 in via equation 3.3.

$$L_{repair} = D_{defect} + 2L_{over} \tag{3.3}$$

where D_{defect} is the diameter of the defect.

3.4 Derivation of Design Equations

As mentioned in section 1.2, defects traditionally fall into either leaking or non-leaking categories. Repairs designed for non-leaking defects use a maximum allowable stress approach on the remaining wall thickness. Alternatively, repairs designed for leaking defects use a fracture based design approach. This section focuses on the derivation of the design equation for leaking pipes.

The derivation begins with an extension of Griffith's quasi-static crack propagation model shown below in Equation 3.4 [21].

$$\gamma = \frac{\delta(W_d - U)}{\delta A} \tag{3.4}$$

This relationship shows that the critical energy release rate, γ, is a function of the work done, W_d, stored internal elastic energy, U, and the differential crack area, δA. The critical energy release rate can be thought of as the energy required to increase the total crack area, A, by an amount of δA.

The total external work done is the internal pressure times the displaced crack volume caused by the internal pressure, shown in Equation 3.5. Internal strain energy is calculated using a linear energy model based on compliance and applied force, shown in Equation 3.6.

$$W_d = PV \tag{3.5}$$

$$U = \frac{1}{2}cP^2 = \frac{1}{2}PV \tag{3.6}$$

where P is the internal pressure load, V is the new volume of the displaced blister, and c is the compliance of the structure. Therefore, the difference in external work and internal energy for bonded structures that exhibit bulk linear elastic behavior away from the crack tip can be expressed in terms of the applied pressure load shown below in Equation 3.7.

$$W_d - U = PV - \frac{1}{2}PV = \frac{1}{2}PV \tag{3.7}$$

Substituting Equation 3.7 into Equation 3.4 yields Equation 3.8.

$$\gamma = \frac{1}{2}P\frac{dV}{dA} \tag{3.8}$$

Equation 3.8 shows that the energy release rate is a function of the constant pressure load and the rate of change of volume with respect to crack area.

Next, Equation 3.8 was applied to a two dimensional pipe with a circular, through wall defect using plate theory. The plate theory model was used in order to obtain a baseline deflection profile of the composite directly above the defect. Figure 3.4 below shows the schematic of the deformed plate above the defect for this problem [21].

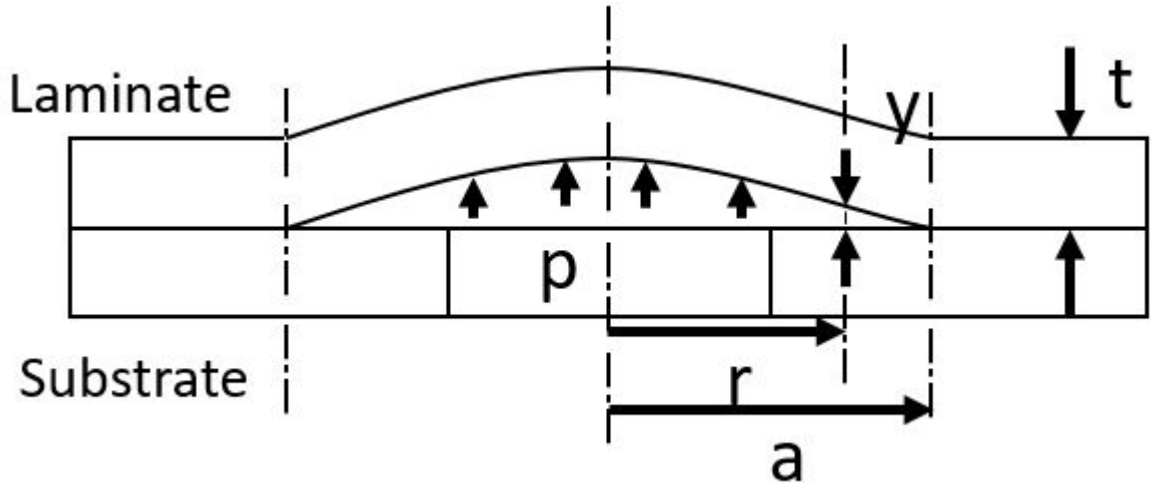

Figure 3.4: Simplified Plate Theory Schematic

The governing equation for the deflection profile of that blister is given in equation 3.9.

$$y\left(r\right)=P\left[\frac{3(1-\nu^{2})}{16Et^{3}}\{a^{2}-r^{2}\}^{2}+\frac{3}{8Gt}\{a^{2}-r^{2}\}\right] \tag{3.9}$$

P = applied internal pressure
ν = effective Poisson ratio
E = tensile modulus of composite repair in the axial direction
t = thickness of the composite
a = radius of circular crack
r = distance from centerline in axial direction
G = shear modulus

where modulus and Poisson ratio are defined as

$$E=\sqrt{E_{a}E_{c}} \tag{3.10}$$

$$\nu^{2}=\nu_{ca}^{2}\frac{E_{a}}{E_{c}} \tag{3.11}$$

with a and c subscripts corresponding to axial and circumferential directions, respectively.

There are a few important assumptions made in this simplified model. First, the defect is assumed to be small in comparison to the plate, which indicates that all displacements and stresses are generated only through bending. Second, since this is a 1D axisymmetric problem, all crack growth occurs evenly around the center of the defect, resulting in a larger, circular flaw. This assumption could lead to an underestimation of deflections if one orientation of the reinforcing fabric is significantly more compliant than the other. This potential error is mitigated by the use of a mixed modulus as shown in Equation 3.10. Lastly, the plate is assumed to be flat and rigid, which indicates that all curvature is ignored.

Using the plate theory model, Equation 3.7 can be rewritten in terms of the displacement profile in Equation 3.12

$$W_d - U = \frac{1}{2}PV = \pi \int_0^a Py(r)rdr + U \tag{3.12}$$

Equation 3.12 shows that the difference between work done and internal strain energy is equal to the product of internal pressure and the rate of change in volume of the blister plus an additional strain energy term. In order to account for thick laminates, this additional strain energy term on the right-hand side of the equation is necessary. This is due to the fact that laminate deflection tends to zero as laminate thickness, t, gets large. In this case, the blister can be modeled as an internally pressurized penny shaped crack [22]. The stored energy for this case combined with Equation 3.12 results in the total difference between external work done and internal stored energy shown in Equation 3.13.

$$W_d - U = \pi \int_0^a Py(r)rdr + \frac{4(1-\nu^2)}{3E}P^2a^3 \tag{3.13}$$

Inserting Equation 3.9 into Equation 3.13 yields Equation 3.14 below

$$W_d - U = \pi P^2 \left[\frac{3(1-\nu^2)}{16Et^3} \frac{a^6}{6} + \frac{3}{8Gt} \frac{a^4}{4} + \frac{4(1-\nu^2)}{3\pi E} a^3 \right] \tag{3.14}$$

In order to get a direct relationship between energy release rate and the material properties, Equation 3.15 below is introduced which represents the change in crack area with respect to crack radius.

$$dA = 2\pi a da \tag{3.15}$$

Lastly, Equations 3.15 and 3.14 are substituted back into Equation 3.8 which yields the final design relationship Equation 3.16

$$\gamma = P^2 \left[\frac{(1-\nu^2)}{E} \left\{ \frac{3}{32t^3} a^4 + \frac{2}{\pi} a \right\} + \frac{3}{16Gt} a^2 \right] \tag{3.16}$$

The energy release rate design formula shown above consists of two separate terms. The first term on the right-hand side represents mode I fracture energy and the second term represents mode II fracture energy. The degree to which each component contributes to overall crack growth depends on the material properties of the laminate as well as defect geometry [21].

In industry, it is often helpful to design repairs strictly in terms of internal pressure and defect diameter, d. This is easily achieved by assuming that pressures exceeding the critical pressure calculated in Equation 3.16 will cause a crack to advance, resulting in immediate failure. Substituting Equation 3.17 into Equation 3.16 and solving for internal pressure yields the desired relationship shown in Equation 3.18.

$$a = \frac{1}{2}d \tag{3.17}$$

$$P = \sqrt{\frac{\gamma}{\frac{(1-\nu^2)}{E}\left\{\frac{3}{512t^3}d^4 + \frac{1}{\pi}d\right\} + \frac{3}{64Gt}d^2}} \tag{3.18}$$

If the value of γ is known, the repair thickness, t, is simply calculated using Equation 3.18 for a given leaking defect. As this is a model based on rigid plate theory, it is interesting to note that pipe diameter does not influence the design of composite repairs using this method.

3.5 Plate Theory Profile Comparison to FEA

The displacement profile generated from this model is approximately parabolic in shape and deflects a maximum of 0.02mm at its peak as shown in Figure 3.5. This profile assumes that the plate is clamped with pinned edges as its boundary conditions.

Next, this plate theory profile was directly compared to a profile extracted from an FEA simulation of a pipe with a full-encirclement repair. It should be noted that the FEA simulation does not include a rigid substrate and takes curvature into account when calculating displacements. Thus, in order to compare these two profiles more closely, steel substrate deflections were subtracted from composite displacements in an attempt to mitigate the effects of a nonrigid substrate. The result is shown in Figure 3.6.

The plate theory model predicts much larger displacements than the FEA model with a 59% difference at their peaks. This difference could be attributed to the fact that the plate

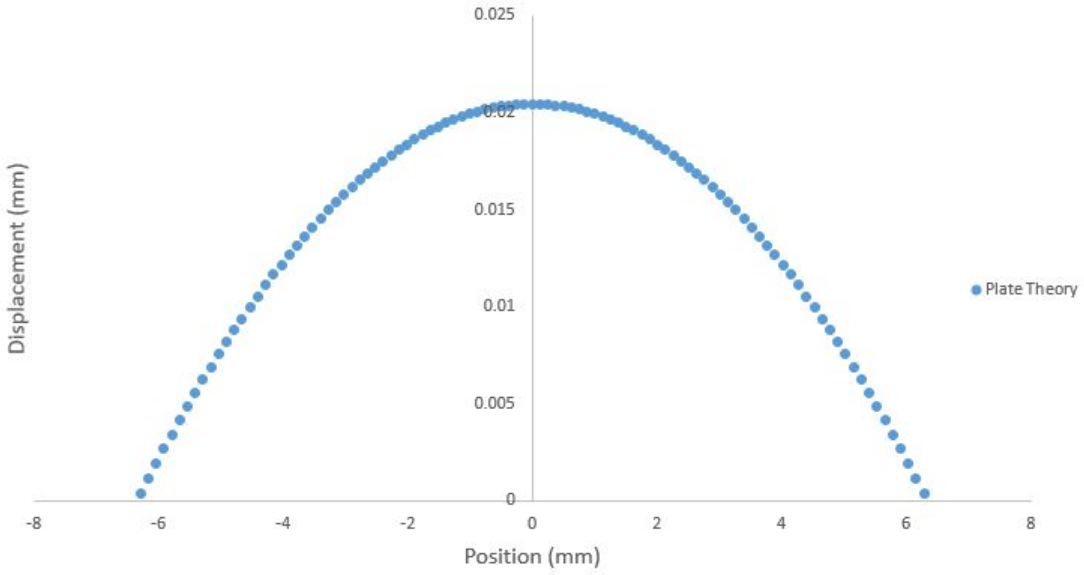

Figure 3.5: Displacement profile generated from plate theory

theory model is limited to 2-dimensions and does not take into account the anisotropic nature of the composite. Additional discrepancies between models could be a result of the simplifying assumptions in the plate theory model.

3.5.1 Pressure Ramp Study

In order to better understand the strain response of the repair during fatigue loading, a pressure cycle was simulated using FEA. Pressure amplitude was increased linearly from 0 psi to 500 psi and the maximum strain in the composite was extracted. These simulations were run with a repair thickness of 0.25 in and an L_{over} of 5.55 in from equation 3.1. The result of the simulation is shown below in Figure 3.7.

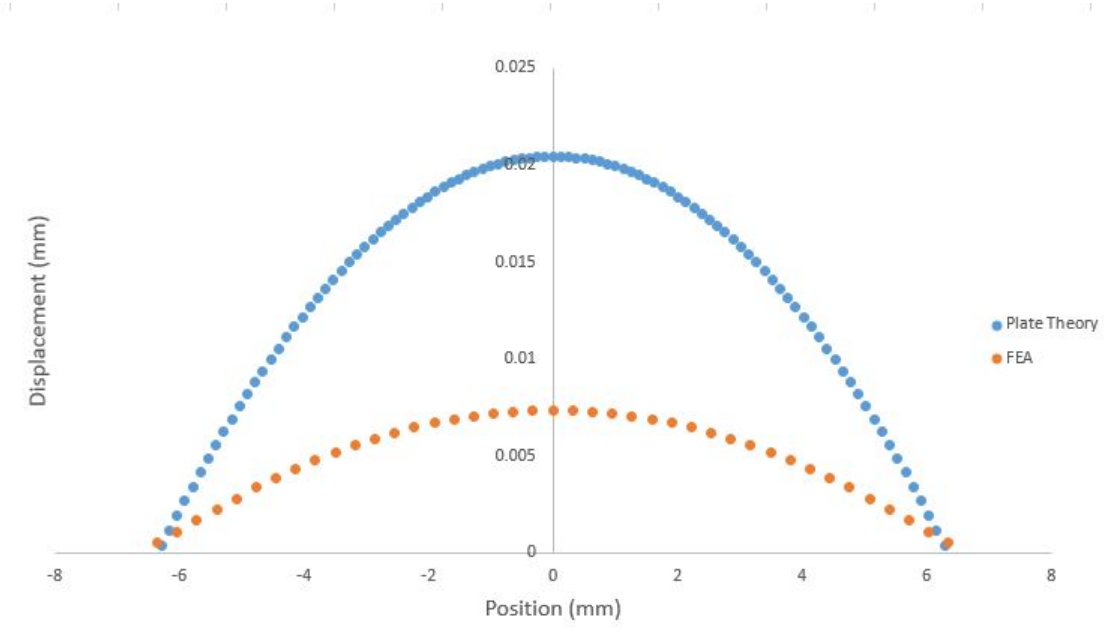

Figure 3.6: Comparison of FEA and plate theory displacement profile

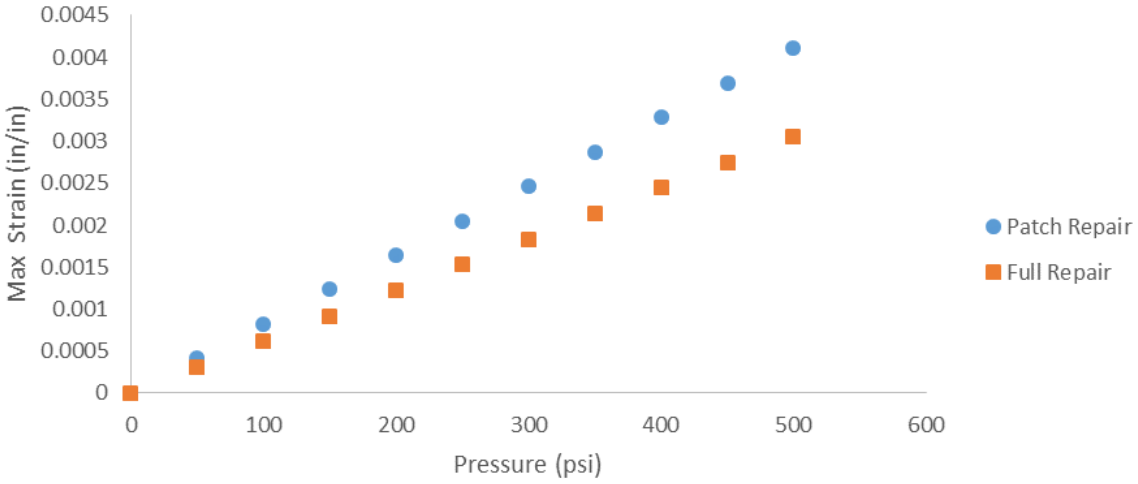

Figure 3.7: Comparison of pressure ramp between patch and full-encirclement repairs

Strain levels in both repair types increase with increasing pressure, as expected. The strain response in the composite is perfectly linear because the applied loading remained entirely elastic. The patch repair exhibited slightly higher strains than the full-encirclement repair with the difference increasing as pressure increases. At the maximum pressure of 500 psi there was a 29% difference between strains in the patch and full repairs. The higher strain levels in the patch repair could be a result of decreased contact surface area with the substrate. This is particularly likely in the FEA simulation since the repair is perfectly bonded to the substrate.

Figure 3.8 below shows where the maximum strain in the composite was located. In the figure, the steel substrate has been removed in order to better show the distribution of strains around the defect. As expected, the largest strain in the repair is located at the edge of the defect where the repair is directly exposed to internal pressure. Additionally, the expanding strain distribution along the bottom surface of the repair indicates that the repair will likely fail due to interfacial delamination before bulk composite failure.

3.5.2 Extent of Repair Study

The extent of the repair, referred to as L_{over}, is the minimum specified distance that the repair must extend axially beyond the damaged section of pipeline as described earlier in section 3.3. In order to understand how the extent of the repair affects the performance of each repair type, L_{over} was varied from a minimum value of 5.55 in, as calculated from 3.1, to 12 in. Figure 3.9 below shows the results of this study.

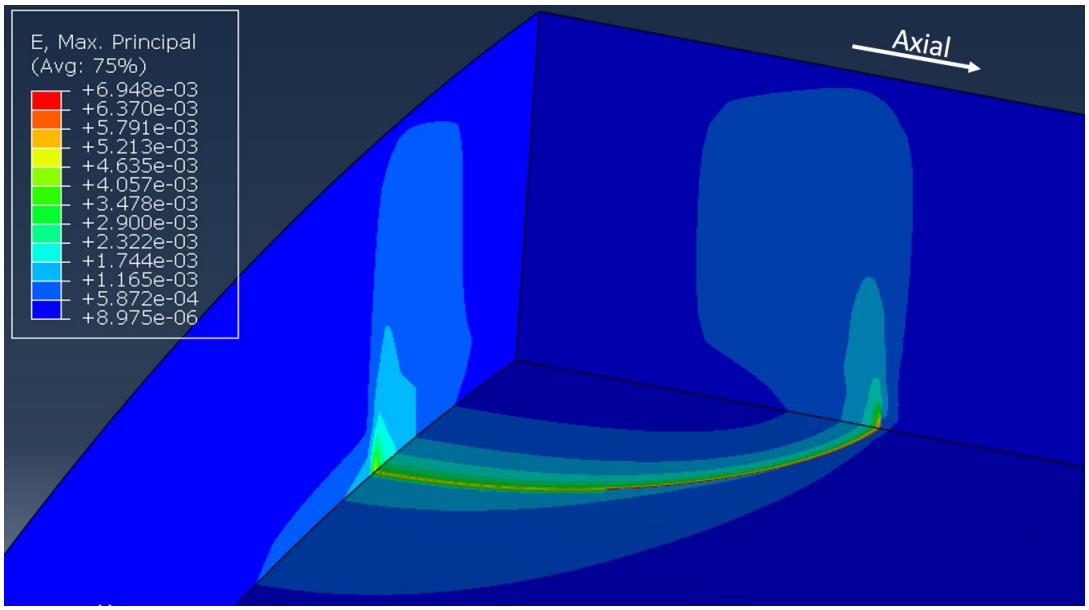

Figure 3.8: FEA showing strain distribution in the composite repair

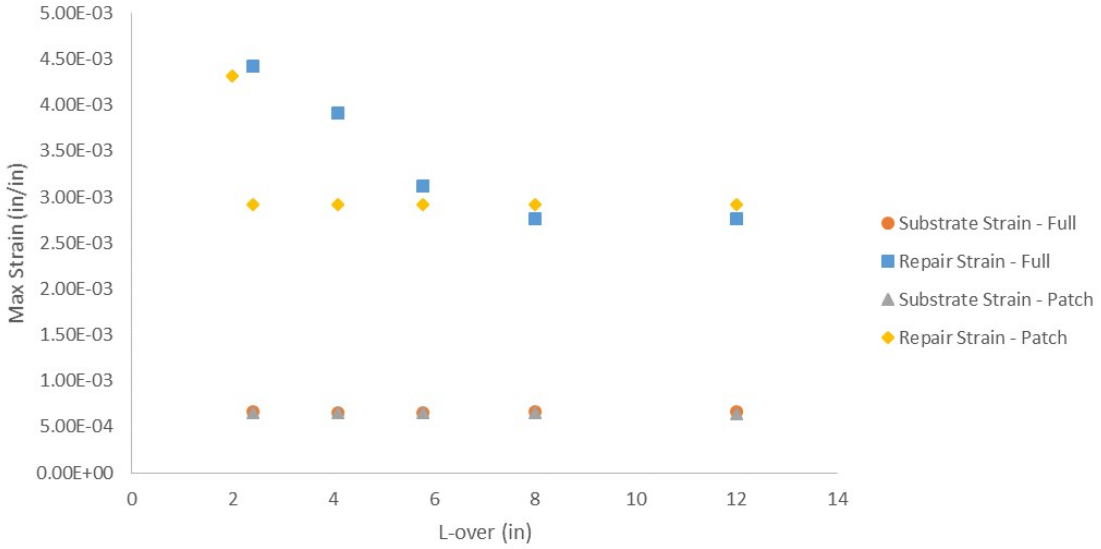

Figure 3.9: Max repair strain as a function of L_{over}

As shown above, exceeding the minimum value of L_{over} does not have a significant effect on the maximum strain levels in the repair. This behavior can likely be attributed to the assumed perfect bond between the composite repair and the substrate in these FEA simulations.

Chapter 4

Experimental Setup

Fatigue testing was performed for all specimens in an effort to characterize the performance of patch and full-encirclement repairs. This chapter describes sample specifications, fatigue testing methods, and instrumentation.

4.1 External Participation

In order to closely replicate repairs that are used in industry, three external pipeline repair companies installed the repairs used in this study. This ensured that all repaired specimens were realistic and that no errors arose from inexperienced installers performing the repair. The three external companies who participated in this study will henceforth be referred to as Company A, Company B, and Company C. Each of these companies was asked to install a total of 6 FRPC repairs, 3 full-encirclement and 3 patch repairs. Additionally, each company was asked to at minimum comply to ASME PCC-2 standard for their repairs in an effort to maintain consistency among specimens. As ASME PCC-2 does not currently

allow for patch-type repairs, all companies simply modified their full-encirclement repair by creating a discontinuity in the circumferential direction when installing their patch repairs. Approaches varied among companies with each company using their own proprietary repair techniques.

4.2 Sample Design & Manufacturing – Small Scale

4.2.1 Pipe Material

As mentioned in section 3.1, all specimens were nominal 6 in diameter schedule 40 ASTM 106B pipes. ASME PCC-2 specifies minimum requirements for quasi-static pipe testing such as pipe diameter and length. Currently, the minimum pipe diameter for performance testing is 6 inches and minimum pipe length is six times the diameter plus repair length. As such, these dimensions were used as guidelines for fatigue testing. Table 4.1 below summarizes pipe dimensions for the fatigue specimens.

Table 4.1: Summary of specimen geometry

Characteristic	Pipe Dimension [in]
ID	6.065
OD	6.625
Wall Thickness	0.280
Length	48

4.2.2 Defect Geometry & Location

To model the effect of a through-wall defect, a 0.5 in diameter teflon disk was applied over a 0.25 in diameter through wall hole. This approach created a debond defect that would act like a through-wall defect of similar size. Machining these defects consisted of simply drilling 0.25 in diameter holes in all the specimens and applying a 0.5 in diameter Teflon disk directly over the drilled hole.

Hemispherical end caps were welded to each end of the specimens as well as inlet and outlet couplings. Figure 4.1 below shows the schematic of a completed pipe specimen after fabrication and welding.

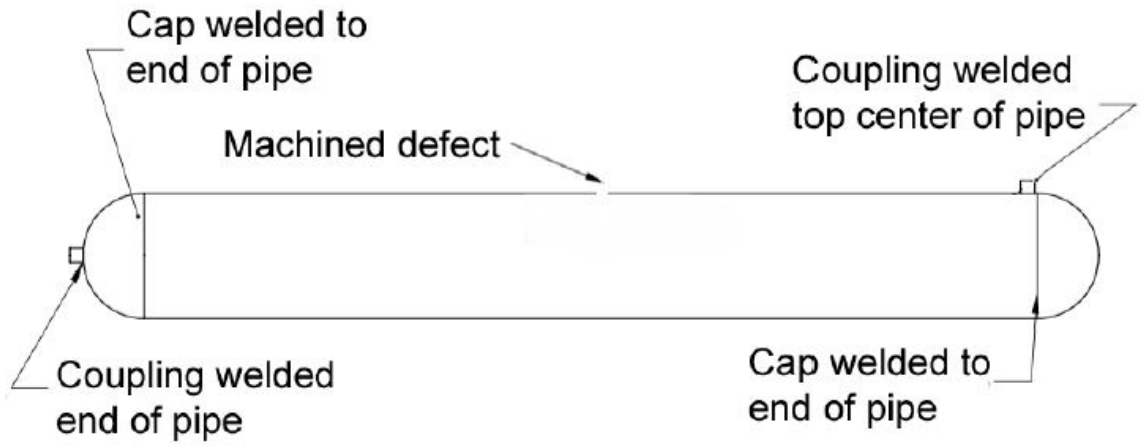

Figure 4.1: Schematic of completed pipe specimen

4.3 Sample Preparation & Manufacturing – Large Scale Testing

The initial project was planned to use a donated 60 inch test vessel for the large scale test phase of this research. Unfortunately, prior to the start of this testing phase, those test vessels were scrapped and were unavailable. As a replacement, a 42-inch vessel was fabricated locally to replace those scrapped vessels. The replacement vessel was fabricated using a 42 inch OD pipe section with welded elliptical heads. After the vessel was welded, the through-wall defects were fabricated by drilling 0.25 in holes in the pipe wall at selected locations. Dimensioned drawings of the large scale test specimen are located in Appendix B.

4.4 Composite Repair Installation

Each of the 3 companies that installed repairs complied to ASME PCC-2 [17] and used their own proprietary materials. Table 4.2 below summarizes each company's repair materials.

Table 4.2: Summary of repair materials per company

	Reinforcing Material		Thermoset Material
	Hoop Direction	Axial Direction	
Company A	Carbon Fiber	Carbon Fiber	Epoxy
Company B	Carbon Fiber	Fiberglass	Epoxy
Company C	Fiberglass	Fiberglass	Polyurethane

The variation in composite materials between companies led to significant differences

in the repair thicknesses. Table 4.3 below shows the average repair thickness and the total number of composite reinforcing plies used to achieve that thickness.

Table 4.3: Summary of repair thicknesses per company

	Number of Plies		Repair Thickness (in)
	Full-Encirclement	Patch	
Company A	6	6	0.135
Company B	17	17	0.44
Company C	6	6	0.125

Another design metric that varied between companies was L_{over}. To ensure that all companies met the minimum testing standard, Equation 3.3 was used with the physical measurements shown in Table 4.4 below.

Table 4.4: Average repair length per company

	Axial Repair Length (in)	
	Full-Encirclement	Patch
Company A	6.625	6.625
Company B	25.75	25.75
Company C	19.25	19.25

Each company met or exceeded the minimum L_{over} as stipulated by PCC-2. Companies B and C exceeded the requirement by more than 6 inches each while Company A exceeded the requirement by only 0.4 inches.

4.5 Fatigue Testing

4.5.1 Flow Loop

In an effort to minimize fatigue testing time, a system was built that could simultaneously test multiple specimens. The fatigue testing consisted of pressure cycling the repaired specimens from 0 to 500 psi at an average rate of 40 cycles per minute. Care was taken to avoid cycling the specimens near their resonant frequency. A schematic of the flow loop is shown below in Figure 4.2.

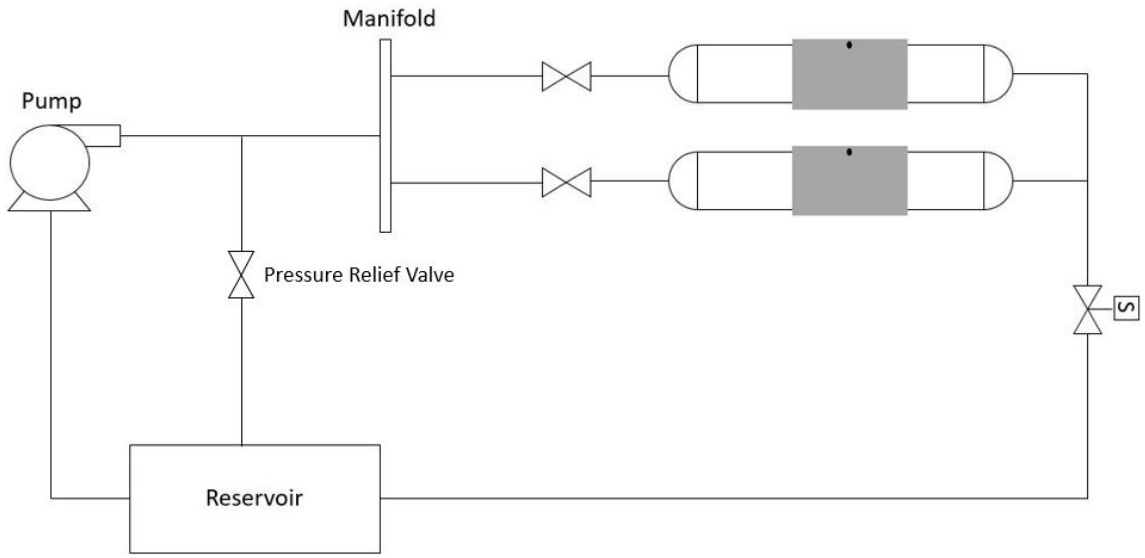

Figure 4.2: Schematic of fatigue system flow loop

The first step in the fatigue testing process was to completely fill the repaired specimens with water and remove all air from the system. Next, the pump was turned on, the pressure relief valve was closed, and fatigue cycling began. Care was taken to ensure that all pipes were secured and tested in a similar manner to minimize external and environmental

factors.

4.5.2 Control System & Cycling

The first component in the control system was an electronic pressure switch that determined the set point for the system. This switch controlled an electromechanical relay that was connected to an analog counter and solenoid valve. The wiring diagram for this control setup can be seen in Figure C.1. The fatigue cycling process began with the pump pressurizing the repaired specimens to the specified pressure of 500 psi. Once the set point pressure was reached, the pressure switch would activate the relay, which applied power to the normally-closed solenoid valve. Once open, the high-flow valve allowed water to return back to the reservoir and depressurize the system. Once pressure in the system dropped to the reset pressure of the electronic switch, the relay would stop sending power to the solenoid valve and the process would begin again. Additionally, the analog counter was wired such that it would trigger with each closing of the solenoid valve, thus providing a counter for fatigue cycles. Lastly, a digital output signal was wired in to provide data to a LabVIEW program. Data acquisition will be discussed in the next section.

4.6 Data Acquisition & Instrumentation

Cycles to failure were recorded for all specimens, however, internal pressure and strain were only recorded for a single patch and full-encirclement repair for each company. In total, 18 samples were tested, but only 6 were instrumented with strain gages. A LabVIEW program was used to record internal pressure, strain, and cycles to failure for those 6 specimens.

4.6.1 Cycle Counting Methods

As mentioned in section 4.5.2, an analog counter was used to record total cycles for all specimens. The analog counter was more reliable than a LabVIEW program that identified pressure peaks in real time. Additionally, the analog counter ensured that data would never be lost due to a power outage. Fatigue cycles for the specimens instrumented with strain gages were counted both using the analog counter and a LabVIEW program. LabVIEW read a digital signal from the control box each time the solenoid was engaged. This signal triggered the computer to record pressure and indicated a peak for that cycle. Each of these peaks was counted as 1 cycle and all cycles were tallied at the end of testing. When compared directly, total cycle count from the analog counter and LabVIEW varied slightly. For all 6 samples instrumented with strain gages, LabVIEW recorded more cycles than the analog counter. It was determined that noise in the digital signal was causing duplicate peaks to be recorded. However, the difference between the final two cycle counts was significantly less than 1% for all specimens and the additional LabVIEW cycles were discarded.

4.6.2 Internal Pressure

Internal pressure was recorded for the 6 specimens instrumented with strain gages using an Omega PX-429 high accuracy pressure transducer. The transducer was calibrated with a 5-point NIST calibration to ensure accurate readings.

4.6.3 Strain Gages

As mentioned earlier in 4.6, one patch and full-encirclement repair from each of the three companies were instrumented with strain gages. For these 6 specimens, strain was recorded for the entirety of fatigue testing. Figure 4.3 below shows the various locations where gages were applied for each repair type.

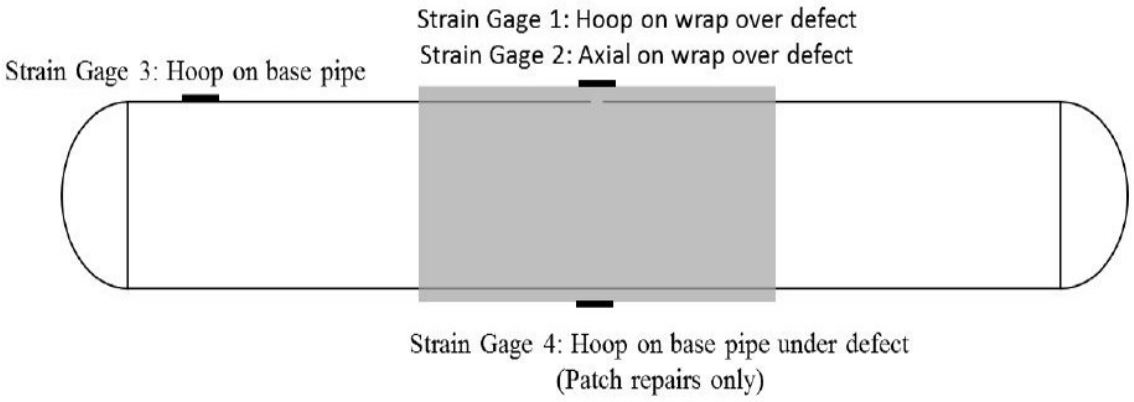

Figure 4.3: Strain gage application locations

As shown above, gages were applied on the surface of the repair directly above the defect, on the base pipe, and, in the case of patch repairs, directly below the defect in the discontinuous section of the repair. Strain gages 1 and 2 were installed at least 48 hours after repair installation to allow for complete curing of the repair. These gages measured strain in both the hoop and axial direction on the surface of the repair. Strain gage 3 measured strain in only the hoop direction for the base pipe. Care was taken to install this gage a sufficient distance from the repair and end cap to record accurate data. Strain gage 4 also only measured strain in the hoop direction and was only applied to specimens with

patch repairs.

Two different types of strain gages were applied to the 6 specimens. In the case of gages 3 and 4, only hoop strain was of interest, so a single axis gage was applied. However, since space directly above the defect on the surface of the composite was limited and both hoop and axial strains were of interest, a biaxial gage was applied to record strains 1 and 2. Both types of gages are shown below with dimensions in Figure 4.4.

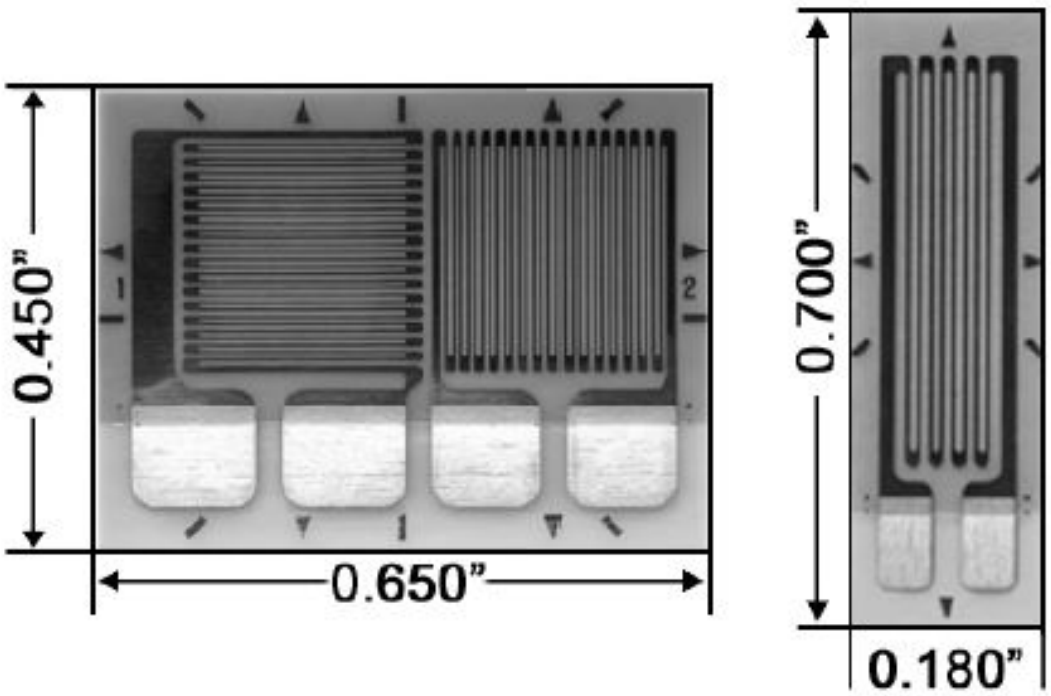

Figure 4.4: Single axis and bi-axis gages used for testing

Each strain gage had a 350Ω nominal resistance with 10V excitation. The gages were connected using 30-gauge wire to a 350Ω National Instruments (NI) quarter bridge completion adapter. These adapters were connected to NI 9237 analog input modules via RJ50

cable. Two NI 9237 modules were used to read strain data, an NI 9222 was used to read internal pressure, and an NI 9401 module was used to count the digital input signals for cycle counting. All four of these modules were connected to a single NI chassis for data acquisition.

4.7 LabVIEW Data Acquisition

A LabVIEW program was used to measure internal pressure, strain, and fatigue cycles for the 6 of the 18 specimens. As mentioned in Section 4.6.1, this program was triggered via a digital output signal from the control system. Upon receiving this signal, LabVIEW would read a single value for each strain gage, the current pressure, and add a cycle to the total cycle count. Additionally, this program was designed such that every 200 cycles it would record 4 full loops of pressure and strain. This allowed for close monitoring of the system to ensure that it was pressure cycling properly and also that all strain gages were still active and reading good data. Figure 4.5 below shows a representative set of loop data.

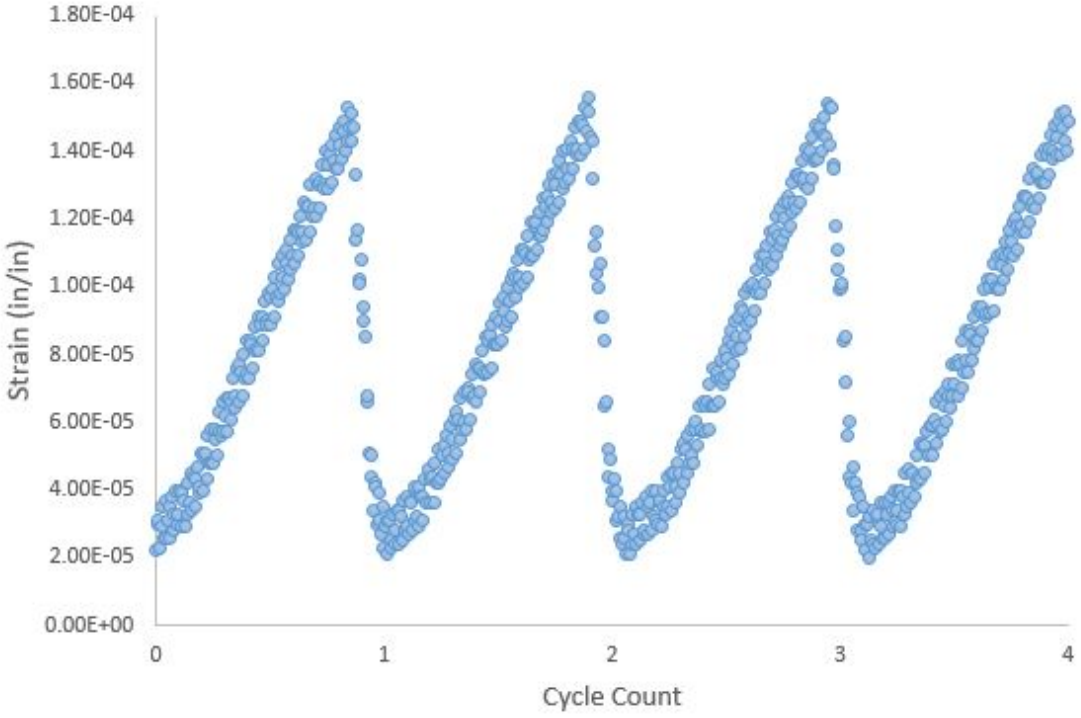

Figure 4.5: Strain loop data

Chapter 5

Experimental Results

This chapter discusses the fatigue data obtained from the 18 tested specimens as well as the strain data obtained from the 6 specimens instrumented with strain gages. Additionally, a comparison between strain data obtained from strain gages and digital image correlation (DIC) will be discussed in detail.

5.1 Fatigue Cycles to Failure

Total fatigue cycles were recorded via the analog counter wired into the control box as discussed in Chapter 4. Failure was defined as the cycle in which water penetrated the repair and the specimen could no longer reach the design pressure of 500 psi. All specimens failed in one of two modes, delamination from the substrate or pinhole leaking through the bulk of the composite repair. Ideally, all failures would be delamination failures because that indicates a lack of voids in the composite repair through which water could penetrate. In total there were 3 pinhole failures, 9 delamination failures, and 5 specimens that reached

runout of 100,000 cycles for a total of 17 specimens. One specimen was sand-blasted by an outside agency before it was tested, reducing the anticipated 18 test results to 17. Table 5.1 below summarizes the failure modes for all tested specimens by company.

Table 5.1: Summary of failure modes per company

	Failure Mode		Runout
	Pinhole	Delamination	
Company A	1	5	0
Company B	0	0	5
Company C	2	4	0

Figure 5.1 below depicts the cycles to failure for each type of repair per company along with the average cycles to failure.

Repairs installed by Company A were very consistent in their fatigue performance. The minimum cycles to failure occurred with a patch repair at 9,794 cycles. The maximum cycles to failure occurred with a full-encirclement repair at 18,976 cycles. The average cycles to failure for Company A was 13,041 cycles with a standard deviation of 3,757 cycles. Company A had the lowest average cycles to failure of the three companies that installed repairs. A standard 2-tailed t-test with a 95% confidence interval was calculated using fatigue data from Company A. The results show that patch-type repairs are statistically similar to full-encirclement repairs with a corresponding p-value of 0.968.

All repairs installed by Company B reached the designated runout of 100,000 cycles, giving them the highest average fatigue cycles to failure of the three companies. It is unsurprising that Company B outperformed Companies A & C due to the fact that their installed repairs were significantly larger as outlined in Tables 4.3 & 4.4. Since all speci-

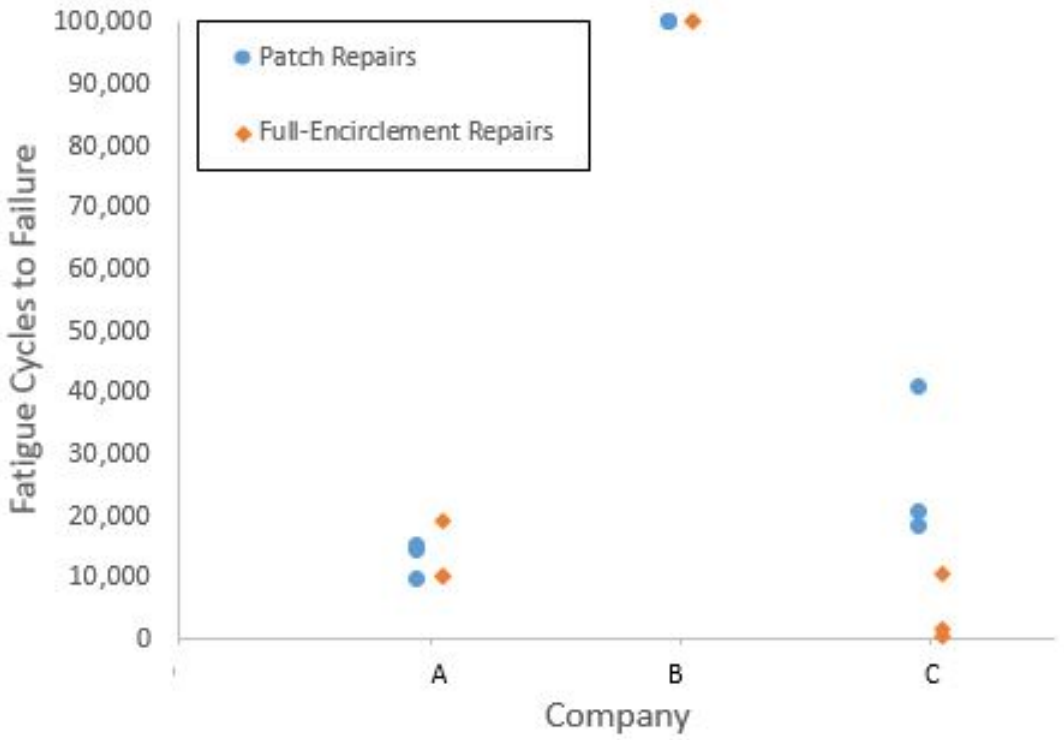

Figure 5.1: Cycles to failure per company

mens reached 100,000 cycles, the average fatigue cycles to failure is 100,000, the standard deviation of the specimens is 0, and, statistically, patch and full-encirclement repairs are similar.

After all the repaired specimens reached runout, they were subjected to a burst test. The results of these tests are shown below in Table 5.2.

Table 5.2: Summary of burst pressures for Company B specimens

Repair Type	Fatigue Cycles	Burst Pressure (psi)
Patch	100,000	3,642
Patch	100,000	3,390
Patch	100,000	3,905
Full-Encirclement	100,000	2,971
Full-Encirclement	100,000	3,597
Full-Encirclement	0	N/A

As mentioned previously, only 5 specimens from Company B were fatigue tested due to an error by an outside agency. The burst pressures for these specimens ranged between 2,971 psi and 3,905 psi and all failures occurred via delamination.

Company C had 5 of their 6 specimens fail at fewer than 20,654 cycles. The final specimen was a patch repair that significantly outperformed the other 5 repairs, reaching 40,948 fatigue cycles. The minimum cycles to failure for Company C was 314 cycles and occurred on a full-encirclement repair. On average, repairs installed by Company C lasted 13,041 cycles and had a standard deviation of 15,116 cycles, the highest among the three companies. A standard t-test was performed with a 95% confidence interval on the fatigue data for Company C. The results indicate that patch repairs are statistically different from full-encirclement repairs with a p-value of 0.03.

Of all the companies who installed repairs, only repairs installed by Company C exhibited a statistical difference between the patch and full-encirclement repairs. This difference is likely due to the significant outperformance of one patch-type repair compared to all other repairs. Performing a 2-tailed t-test with a 95% confidence interval on all fatigue specimens tested shows that patch and full-encirclement repairs are not statistically different with a corresponding p-value of 0.094. As a check, the same t-test was performed

on all fatigue specimens except those that reached runout. This test yielded a p-value of 0.091, indicating there is still no statistical difference between repair types. Thus, fatigue cycles to failure indicate that patch repairs are a viable solution for repairing through-wall corrosion defects in 6-inch diameter pipeline. A complete fatigue summary of all small scale specimens is tabulated in Appendix D.

5.2 Large-Scale Fatigue Results

The large test was initiated after the completion of the small scale tests in case the test results indicated that there were major issues with the basic design approach in PCC-2. The tanks cycled at much lower rates, which required retrofitting the test apparatus in Figure 4.2 with appropriate controls to allow for 24 hour runs. This approach was working well, but at approximately 6,000 cycles the knuckle region of the vessel developed a crack. Stress analysis of the pressure vessel during the design phase indicated that the vessel was safe for the applied internal pressure. However, the solenoid valves were installed on the head and it is likely that the hammering caused when the solenoids opened under pressure caused the failure. This assumption was reinforced when a related test system using a nearly identical vessel and fatigue setup developed a crack in the same region. The vessel was drained and then weld repaired and then testing was resumed. The crack propagated again after approximately 500 cycles. The vessel has been weld repaired four times at this point with each test running for approximately 500 to 1,000 cycles before a new crack is initiated or a weld repair fails by cracking at the end of the repair. The test is ongoing and alternative repair strategies are being investigated. The current cycles on the test vessel is 11,444 cycles.

While this test has not yet reached run out, one experimental observation can be made.

All companies applied the same repair size on the large scale specimen as was applied on the small scale specimen. For the small scale tests, failures in the full-encirclement repairs were observed at approximately 10,000 cycles for both company A and company C. While the test has not proceeded beyond the maximum fatigue cycles of any of the patch or full-encirclement specimens, a t-test implies that the current cycle count, 11,444, is statistically similar to the average failure cycles of the patch ($t = 0.98$) and full ($t = 0.52$) repairs for company A. This is also true for the patch repairs of company C ($t = 2.11$). Based on this, even if the repairs failed on the next cycle, the fatigue life would have statistically similar behavior as the small scale specimens. From this observation, it is likely that the patch repairs installed on the large scale specimen have similar fatigue behavior to those installed on smaller diameter pressure equipment.

5.3 Digital Image Correlation

Digital image correlation (DIC) was performed on one patch and one full-encirclement repair for each company. DIC is a useful tool for computing surface strains by using a random speckling pattern combined with high-resolution cameras. This section describes the process of DIC analysis.

The first step in the DIC process is to apply a thin coat of white paint to the surface of interest, which in this case, was the surface of the composite repair just above the defect. This base coat of paint extended approximately 4 inches in each direction away from the defect. This base coat is allowed to dry and then a speckle pattern is applied to the white surface by carefully spraying black paint over the white. The final pattern was inspected to make sure that the individual speckles were coarse enough to be distinguishable from

each other, but not so coarse as to obscure correlation. An example of a successful speckle pattern is shown below in Figure 5.2.

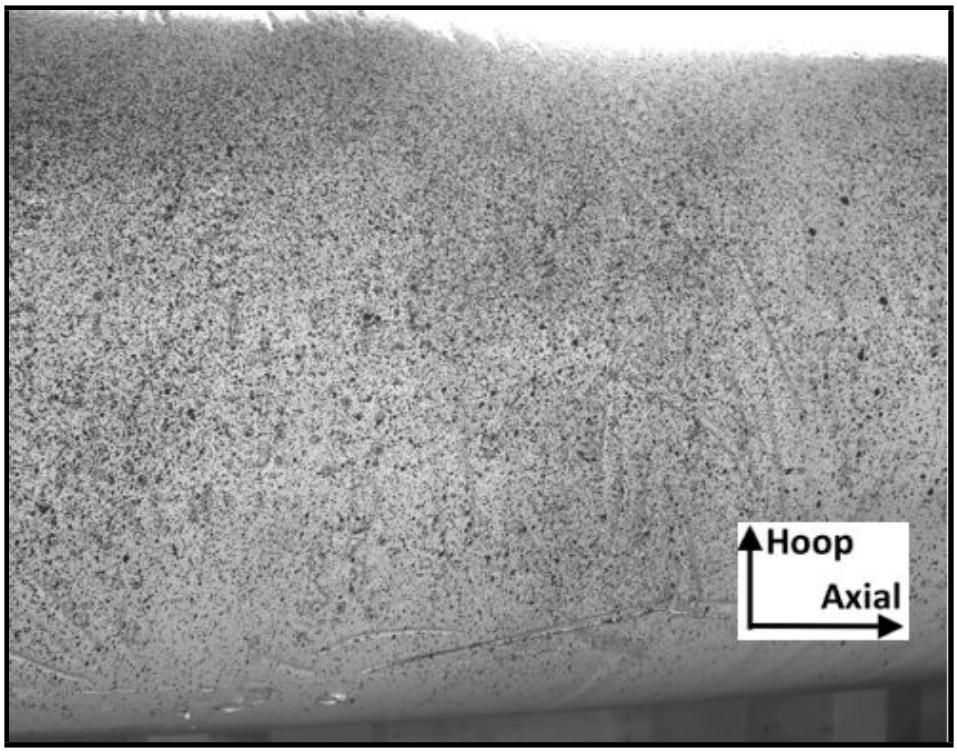

Figure 5.2: An example speckle pattern on a composite repair

After an adequate speckle pattern was applied, the pipe specimen was connected to a manually controlled pump, which allowed for better control of the applied pressure. Next, DIC software and high-resolution cameras were setup at an appropriate distance from the specimen. Due to low lighting in the testing facility, 3 LED lights were also placed in the test room to obtain usable images. Two of the three LED lights were mounted to the tripod directly outside the cameras, while the third light was mounted to the underside of the tripod. This allowed for equal light exposure and the best possible setup for successful

DIC. A schematic of the DIC setup is shown below in Figure 5.3

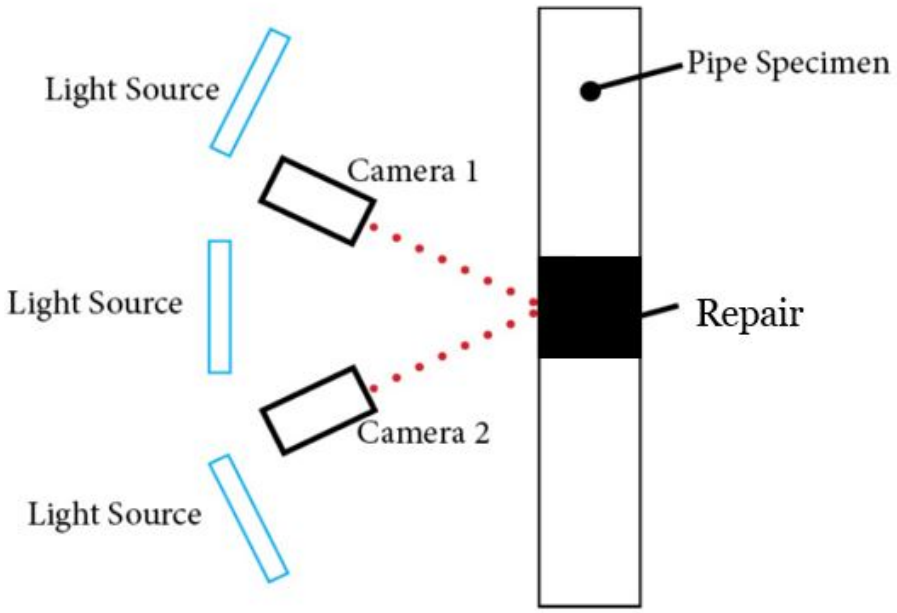

Figure 5.3: DIC setup with high-resolution cameras and LED light sources

After all light sources and cameras were setup properly, each camera was focused on the same area of interest with a wide enough lens to view the entirety of the speckled region. The lens selection was integral to a successful DIC analysis because correlation can only be performed on overlapping regions of images. Once focused, a 9 pixel x 12 pixel grid spaced at 3mm was used to take calibration images. A number of calibration photos are taken at various orientations so that the cameras can identify locations on the speckle pattern. An example of a calibration image is shown below in Figure 5.4.

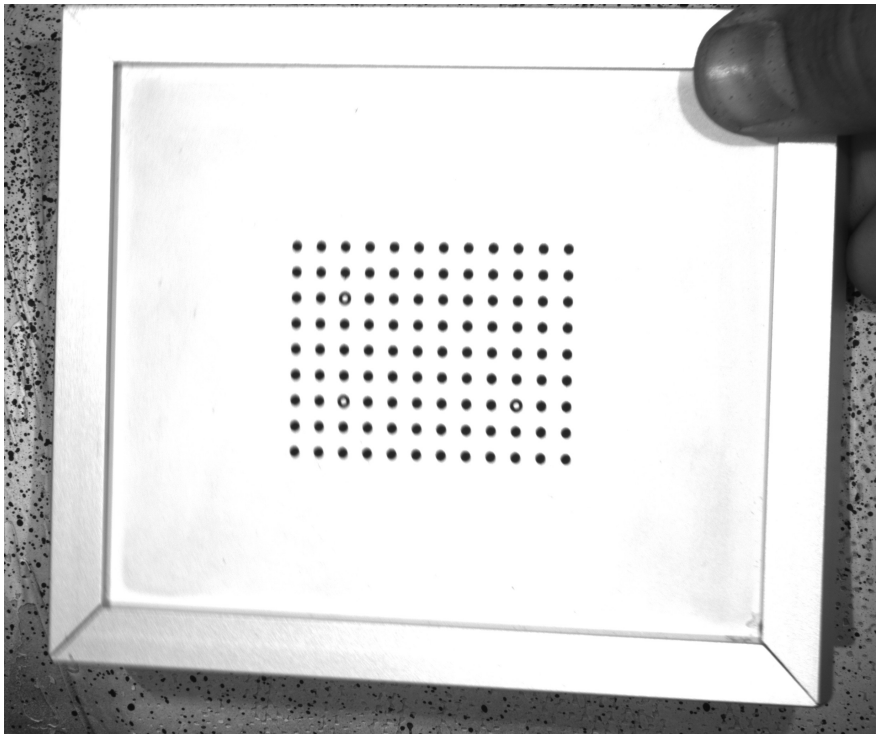

Figure 5.4: An example of a DIC calibration image

After all calibration images were taken, DIC images were taken at discreet pressure intervals of opsi, 250 psi, 375 psi, and 500 psi during pressure ramping. Four images were taken at each pressure interval after the specimen had maintained that pressure for several seconds.

5.3.1 DIC Results

DIC analysis was performed primarily to obtain full-field hoop and axial strain values on the surface of the composite repair. Figure 5.5 below shows a representative DIC strain analysis in the hoop and axial directions for Company C as an example. All DIC analyses

can be found in Appendix E.

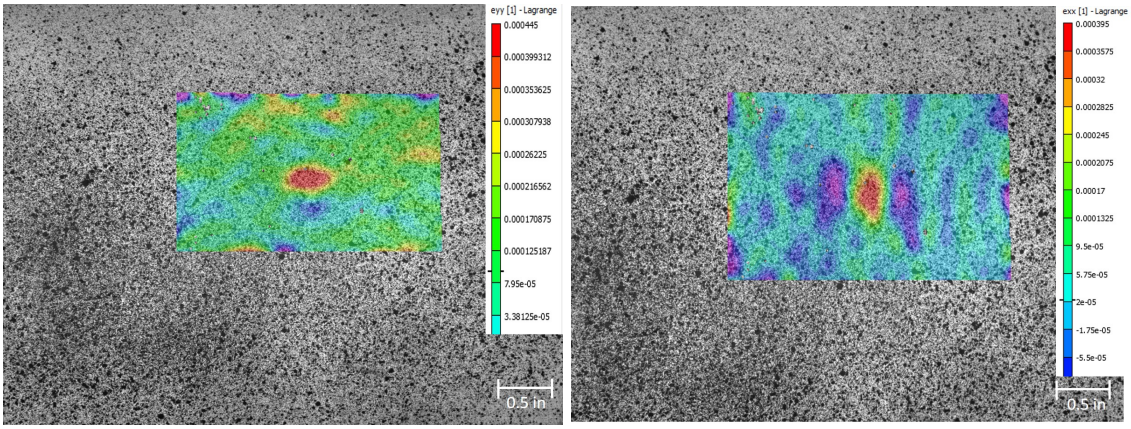

(a) Hoop strains (b) Axial strains

Figure 5.5: DIC analysis of a patch repair installed by Company C at 500 psi

In order to perform DIC analyses, an appropriate area of interest must be defined in which strains will be calculated. To achieve this, the entire speckled region was analyzed and then a smaller area around the defect is reanalyzed. In this case, the area of interest was approximately 2.5 in x 1.75 in.

Figure 5.5a above clearly shows the defect as the circular red area of high strain in the center of the area of interest. For this example, the maximum hoop and axial strains in the composite were 0.0445% and 0.0395%, respectively. Hoop strains rapidly decrease in all directions as the distance from the center of the defect increases beyond the defect edge. This is to be expected as there is no steel substrate to support the composite repair directly over the defect.

Figure 5.5b shows interesting behavior that the surface of the composite repair exhibited when pressurized. The axial strains become compressive just outside of the diameter of the defect, but only in the axial direction. These compressive axial strains were predicted

by the FEA model shown in the red ellipse below in 5.6.

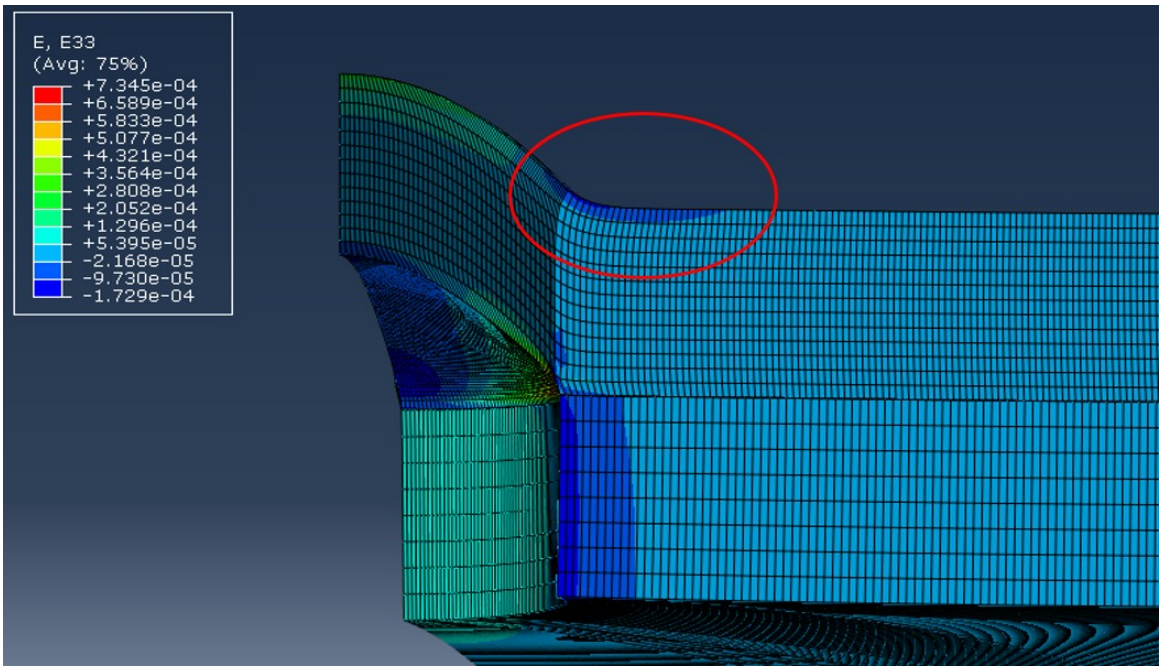

Figure 5.6: FEA model prediction of localized compressive axial strains on the surface of the composite repair

As mentioned previously, the exact values of the FEA model are not as important as the overall trend that it provides. The compressive strains are likely due to the composite repair bending back upon itself as the pressurized blister grows. It is helpful to think of this behavior as a cantilevered beam in bending, as one surface experiences compression and the opposite surface experiences tension.

5.3.2 DIC & Strain Gage Comparison

Another purpose for DIC analysis was to compare the strain values obtained from DIC testing with those obtained from the applied strain gages. Data for these comparisons was

taken from the area directly above the defect where the strain gage was located. In order to avoid local concentrations of strains present in DIC images, an area the size of a strain gage was averaged into a single value, shown below as a black box in Figure 5.7.

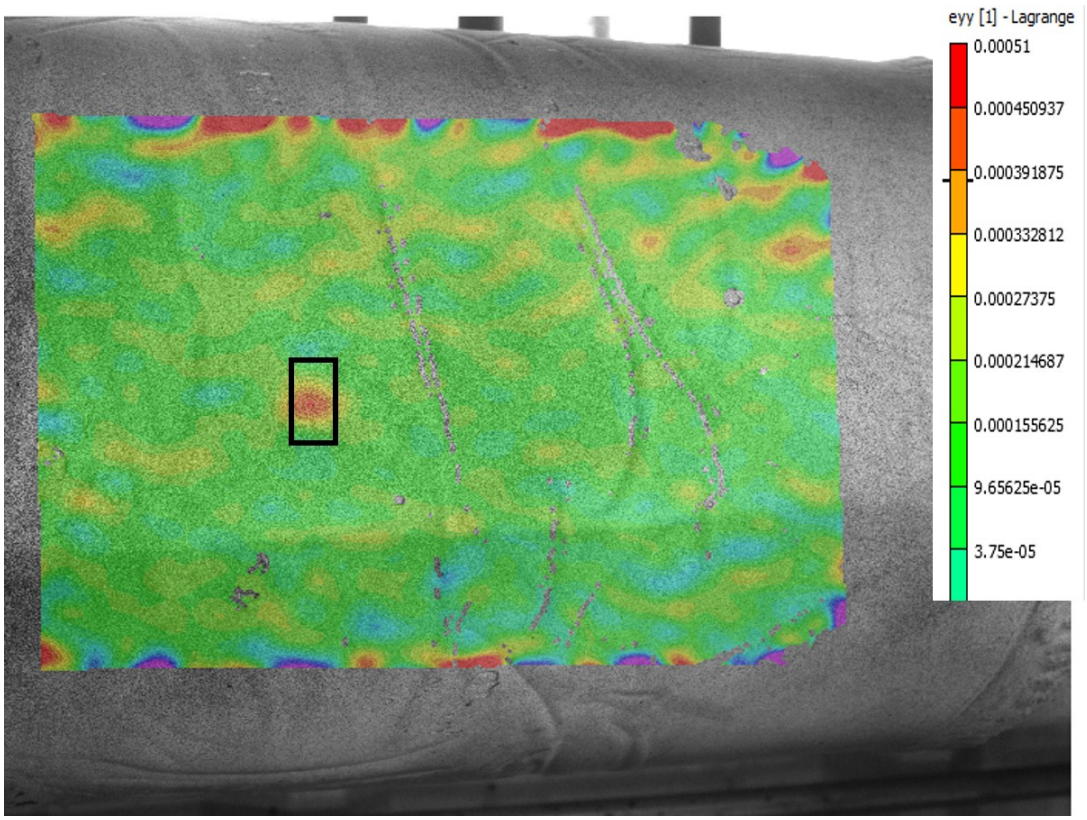

Figure 5.7: Representative DIC from Company A used to determine strains at same location as physical gage represented by the black box

Figure 5.8 below graphically shows the comparison of all DIC strains and strains obtained from the physical gages. It should be noted that due to a data acquisition error, physical strain measurements were not obtained for a patch specimen repaired by Company C.

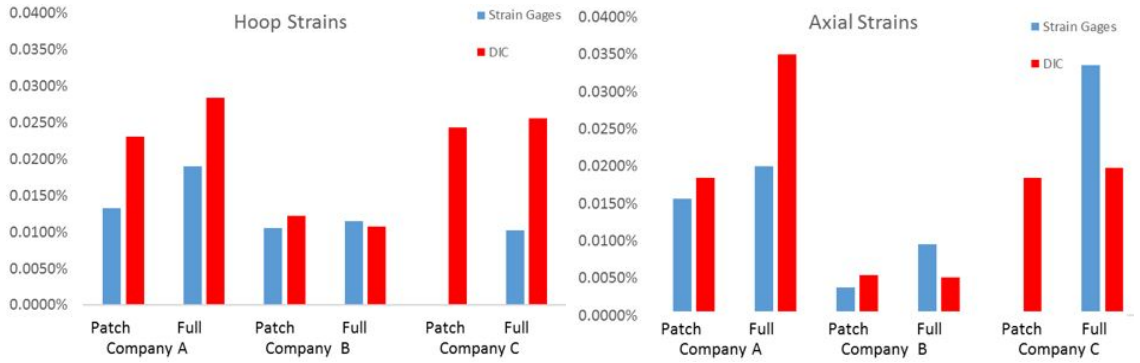

(a) Comparison of hoop strains (b) Comparison of axial strains

Figure 5.8: Comparison of DIC strains vs physical gage measurements

Strains obtained from DIC analysis were consistently larger than those obtained from physical strain gages with the exception of the hoop strain on a full repair from Company B and the axial strain on a patch repair from Company C. In the case of Company B, the percent difference between strains is only 6.3%, which is within the acceptable error of these instruments. For Company C, however, the large percent difference of 51.5% between DIC and strain gage values is likely due to the axial portion of the gage being placed more centrally over the defect. This would also explain the relatively low hoop strain for the same gage as it was not placed directly over the defect.

In all other cases, DIC analysis produced strains that were larger than physical gage measurements. This trend can likely be attributed to slight variation in physical gage placement on the surface of the repair. The companies installing repairs were instructed to take care to keep the defect as centered as possible under the repair to allow accurate gage placement. However, after installation, it was difficult to determine exactly where the defect was located underneath the repair. Thus, gages were carefully applied to the center of the repair to mitigate error.

Since the defect size is relatively small and the biaxial strain gages are large, it is possible that the high strain levels seen just above the defect may not have been properly recorded by some strain gages. An example of this misalignment is shown in Figure 5.9.

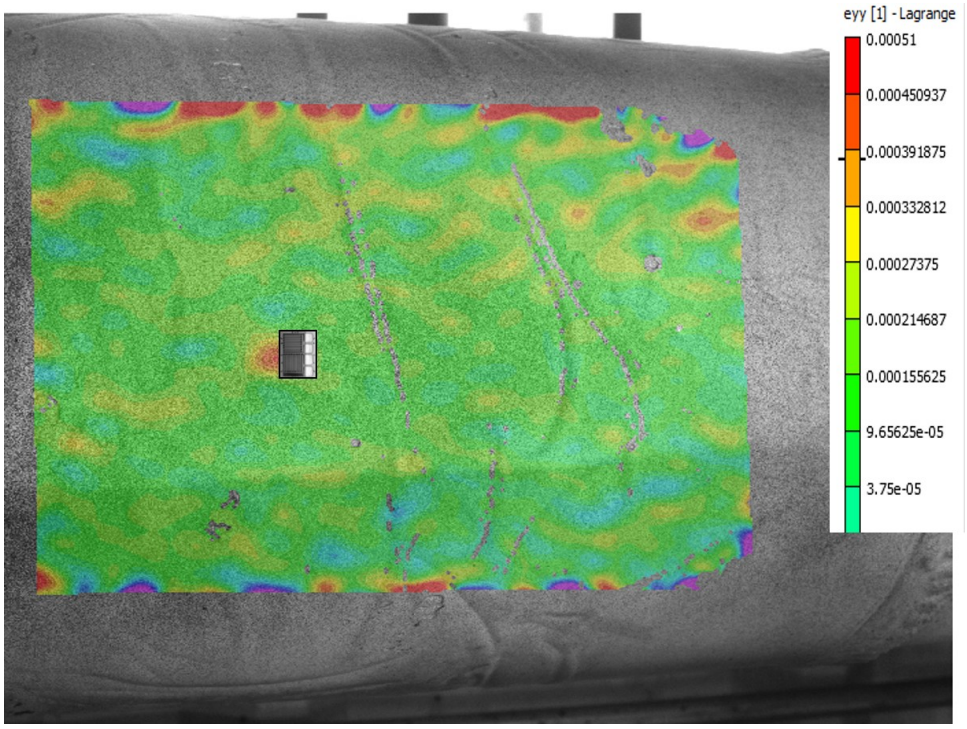

Figure 5.9: Slight misplacement of physical strain gage

Figure 5.9 shows that misplacing a physical gage by only 0.25 in can have significant effects on strain output due to the large strain gradient above the defect. However, even if all gages were perfectly centered directly above the defect, some error would be present in the strain readings because the total area of the strain is divided between hoop and axial sections.

The potential misplacement of strain gages on the surface of the repair led to a gage

placement sensitivity study. In this study hoop strain values were extracted from both the FEA model and DIC image results at discrete angular positions around the repair. In order to make a direct comparison between the theoretical FEA model and the physical DIC measurements, all strains were normalized using the maximum strain directly above the defect from their respective measurement system. The results of that study are shown below in Figure 5.10.

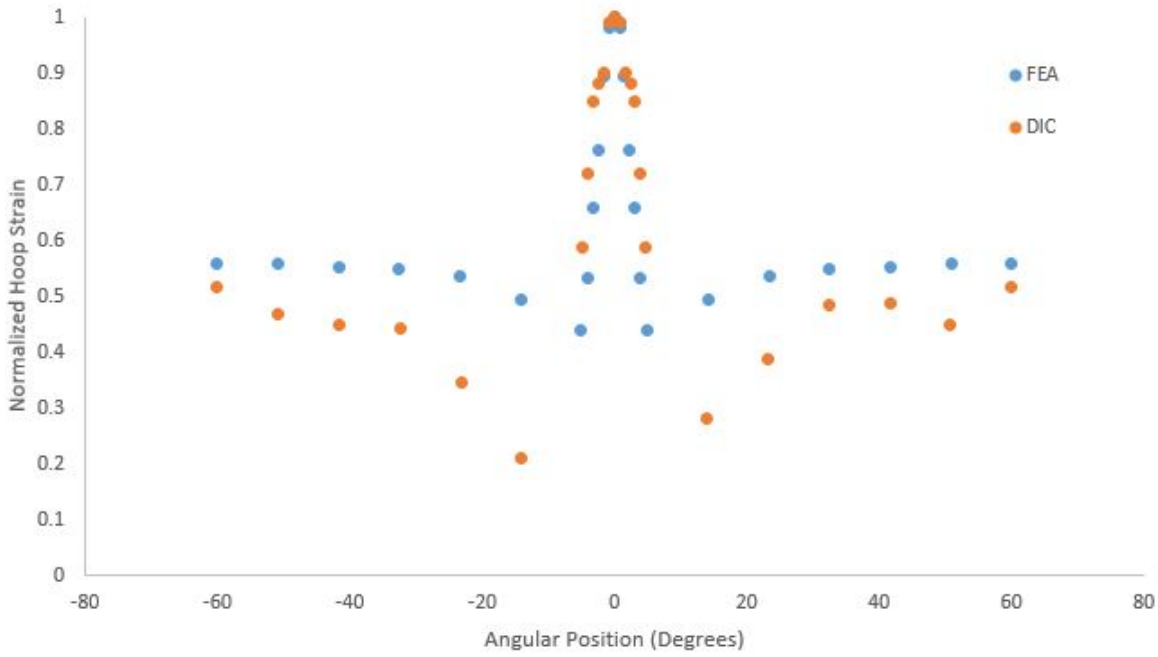

Figure 5.10: Sensitivity study results

As seen in the above figure, the two profiles compare well to each other near the center of the defect, but as distance from the defect increases, hoop strains obtained from DIC are consistently smaller. However, both models were very sensitive to variation in gage placement in the circumferential direction. Variations greater than 5 degrees in either direction

resulted in over 50% reduction in overall hoop strain with the most significant reduction occurring directly outside the defect. This behavior is also present in the sensitivity studies performed in patch repairs using both hoop and axial strains. This sensitivity may have had some effect on the significant differences between hoop strains obtained from DIC and from physical gages placed on the repair surface.

When strains obtained from DIC and physical gages are internally compared, there is little difference between hoop and axial strains. Traditionally, hoop strains are expected to be twice that of the axial strains for orthotropic materials in thin-walled pressure vessels. However, hoop and axial strains could be similar if the stiffnesses in each direction were different by a factor of two. The FEA model shows similar behavior with only a 30% difference between hoop and axial strains on the surface of the repair.

5.3.3 DIC Strain & Plate Theory Comparison

The final purpose of the DIC analysis was to compare out of plane displacement for both patch and full-encirclement repairs against the PCC-2 design equation shown earlier in Equation 3.16. This comparison shows the performance of each repair type relative to the design standard. Figure 5.11 shows the out of plane displacement for a patch repair installed by Company C as an example.

Displacement values were taken on a path indicated by a white line in Figure 5.11 above. Before a direct comparison was made between the DIC and theoretical profiles, substrate displacements were subtracted from the DIC analyses. This was necessary because of the inherent assumption of the design equation that the substrate is rigid. The resulting displacement values were then plotted against the design equation, which is shown below

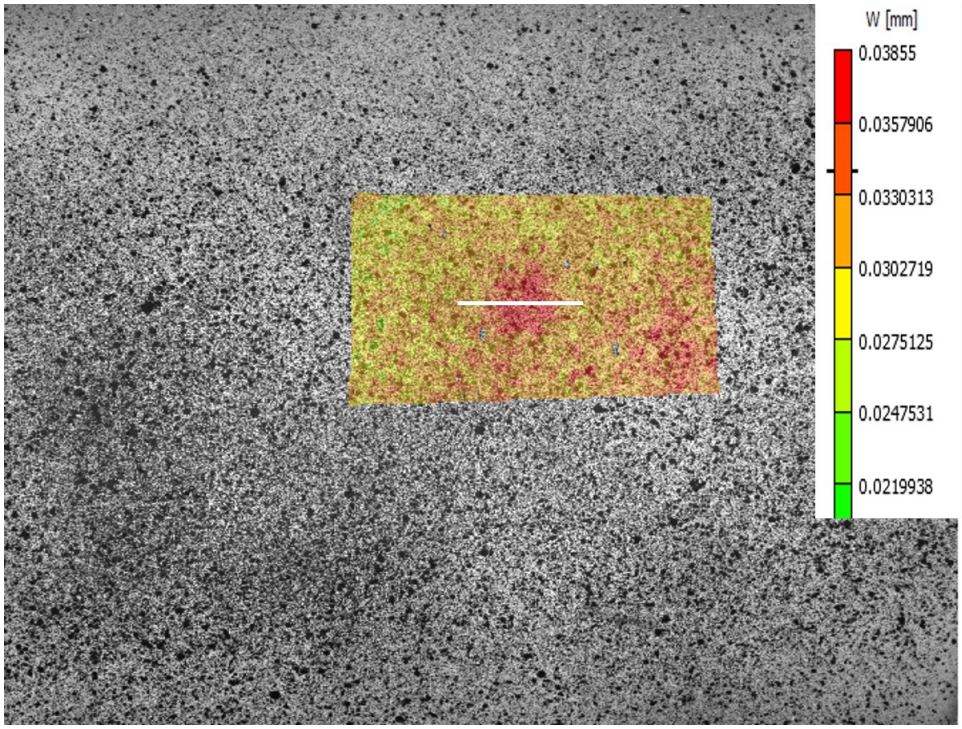

Figure 5.11: Out of plane displacement of a patch repair installed by Company C

in 5.12.

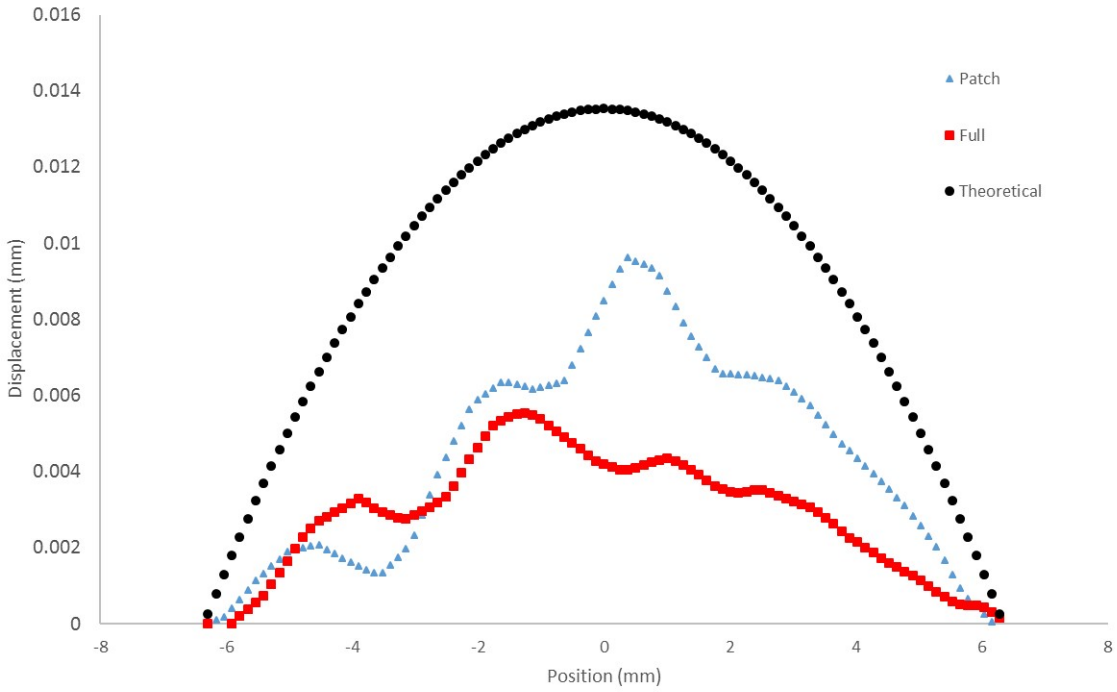

Figure 5.12: Comparison of out of plane displacement for each repair type installed by Company C and plate theory

The theoretical profile exceeds the measured DIC profiles for both patch and full-encirclement repairs. These DIC results imply that the design criteria in PCC-2 for composite repairs is conservative and that patch type repairs are a viable solution for leaking defects on 6-inch diameter pipeline.

5.4 Strain Gage Results

Strain gages were installed on one full-encirclement and one patch repair for each of the 3 companies for a total of 6 specimens. Specimens with full-encirclement repairs were

outfitted with 3 strain gages whereas specimens with patch repairs were outfitted with 4 strain gages. The locations of these gages were shown previously in Figure 4.3 and are shown again below for reference. After fatigue testing was complete, strain values for all gage locations were analyzed.

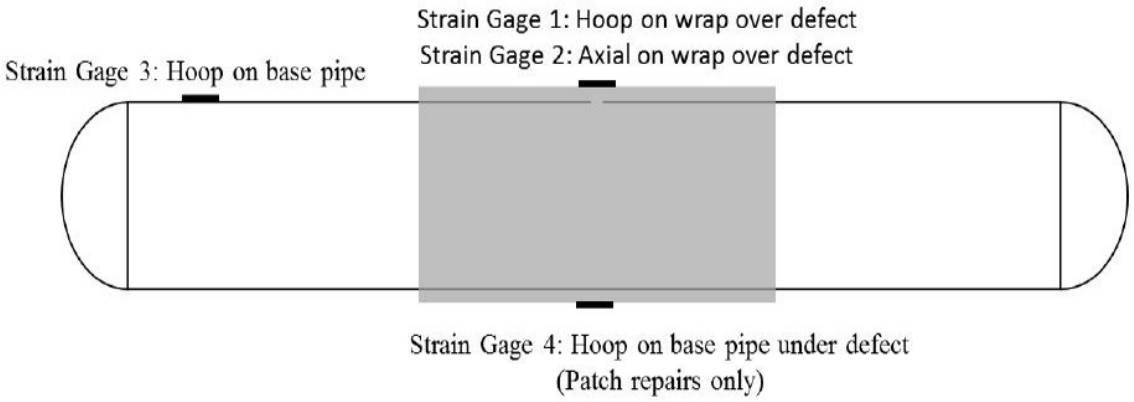

Figure 5.13: Strain gage application locations

5.4.1 Company A

Average strain values were calculated for each installed gage over the entire life of the pipe. These values are tabulated below in Table 5.3 for patch and full-encirclement repairs installed by Company A.

Table 5.3: Average lifetime strains obtained from gages for Company A

Company A - Average Strains over Life				
	Repair Hoop	Repair Axial	Substrate Hoop	Substrate Underside
Full-Encirclement	0.0190%	0.0200%	0.0074%	N/A
Patch	0.0133%	0.0156%	0.0038%	0.0096%

The maximum values of average lifelong strains were observed on the surface of the repair in the axial direction at values of 0.0200% for the full-encirclement repair and 0.0156% for the patch repair. Strains obtained from the full-encirclement repair were consistently larger than strains obtained from the patch repair. This behavior was not predicted by the FEA model and is unexpected. However, post-installation reports from each company stated that more care had to be taken when installing patch repairs to keep them properly oriented. It is possible that this extra caution resulted in slightly better installations with fewer voids, which would result in an overall lower strain.

Average substrate strains for Company A were lower than the expected value of 0.019% at 0.0038% and 0.0074% for patch and full-encirclement repairs, respectively. The estimated value of 0.019% was obtained from the thin-walled pressure vessel equations shown below in Equations 5.1 & 5.2. These results were unexpected and may be partially due to a 12.5% allowable variation in wall thickness for ASTM 106B steel pipe. Estimating hoop strains for a pipe that has 112.5% of the nominal thickness yields a value of 0.017%, which also exceeds measured values.

$$\sigma = \frac{PD}{2t} \tag{5.1}$$

$$\epsilon = \frac{\sigma}{E} \tag{5.2}$$

σ = hoop stress
P = internal pressure
D = pipe OD
t = pipe wall thickness
E = elastic modulus

Next, the behavior of individual gages was analyzed over the entire lifespan of fatigue testing. Figure 5.14 below shows the strains observed at the beginning and end of fatigue testing for both patch and full-encirclement repairs.

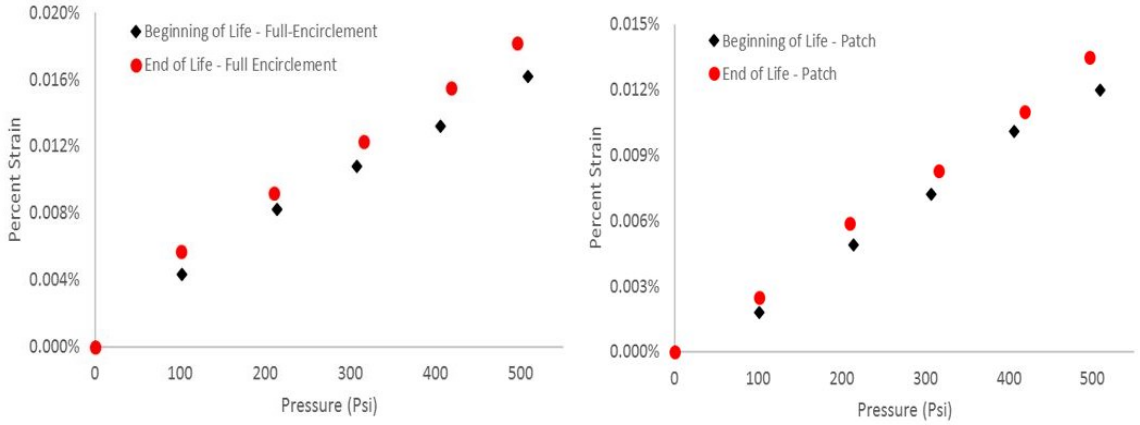

(a) Full-encirclement repair

(b) Patch repair

Figure 5.14: A comparison of repair hoop strains over fatigue life for both repair types installed be Company A

Figure 5.14 above shows that repair hoop strains increase as fatigue cycles increase for both repair types. This trend is observed in both axial and hoop strains obtained from the surface of the repair, but is not present in strains obtained from the substrate. Substrate hoop strains remained relatively constant over their lifetime. This analysis was repeated for all companies and the trend is consistent throughout. The increase in strain as fatigue cycles increase is likely a result of progressive damage in the composite repair.

5.4.2 Company B

The average lifetime strain values for each gage applied to repairs installed by Company B are tabulated below in Table 5.4.

Table 5.4: Average lifetime strains obtained from gages for Company B

Company B - Average Strains over Life				
	Repair Hoop	Repair Axial	Substrate Hoop	Substrate Underside
Full-Encirclement	0.0115%	0.0095%	0.0162%	N/A
Patch	0.0105%	0.0037%	0.0154%	0.0130%

The maximum average strains for Company B specimens were observed in the hoop direction on the substrate at values of 0.0154% and 0.0162% for the patch and full-encirclement repairs, respectively. These values are close to the expected value of 0.019% obtained from mechanics Equations mentioned previously.

Strains from the full-encirclement repair were slightly higher than those obtained from the patch repair. Again, this unexpected behavior may be attributed to extra care during installation or slightly different strain gage placement.

5.4.3 Company C

Average lifetime strains were also calculated for strain gages applied to the Full-Encirclement repair for Company C. These values are tabulated below in Table 5.5. Strain gage measurements were not obtained for the patch repair due to a data acquisition error.

The maximum value of strain was 0.0335% and occurred in the axial direction on the surface of the full-encirclement repair. As mentioned previously, this high strain value is likely due to the axial portion of the strain gage being centrally located directly above the defect. Based on overall trends from DIC and strain gages, it is likely that the patch repair

Table 5.5: Average lifetime strains obtained from gages for Company C

Company C - Average Strains over Life				
	Repair Hoop	Repair Axial	Substrate Hoop	Substrate Underside
Full-Encirclement	0.0103%	0.0335%	0.0109%	N/A
Patch	-	-	-	-

would have had hoop and axial strains slightly less than those of the full-encirclement repair.

5.4.4 Comparison of Repair Types

Strain levels of patch and full-encirclement repairs were compared in an attempt to quantitatively determine repair performance. This comparison consisted of taking the average hoop strains from the surface of the repair for both repair types and calculating the percent difference. This comparison is tabulated below in Table 5.6.

Table 5.6: Comparison of surface repair strains for both repair types

Company	Repair Type	Surface - Hoop	Percent Difference
A	Patch	0.0133%	35.3%
	Full-Encirclement	0.0190%	
B	Patch	0.130%	11.1%
	Full-Encirclement	0.0145%	
C	Patch	-	N/A
	Full-Encirclement	0.0103%	

The percent difference of surface hoop strain between repair types for Company A was 35.3%. This large percent difference may be attributed to slightly different strain gage placement on each repair. Repairs installed by Company B showed only an 11.1% difference between repair types, which indicates that both repairs are developing strain in a similar manner. Lastly, it was not possible to calculate percent difference based on strain

gage measurements for Company C due to a lack of data for their installed patch repair. Performing a two-tailed t-test with an α of 0.05 on all installed patch and full-encirclement repairs yielded a p-value of 0.011. This result indicates that patch and full-encirclement repairs are not statistically different from a surface strain standpoint.

Chapter 6

Conclusions and Recommendations

This research conducted experimental and computational studies of patch and full-encirclement bonded composite repairs applied over simulated through-wall defects. Computational studies included finite element analysis and plate theory models to provide overall trends to be expected in experimental testing. Experimental testing included pressure fatigue testing as well as digital image correlation analysis to quantitatively compare the behavior of each repair.

The FEA model showed that far-field substrate hoop strains were similar for both patch and full-encirclement repairs. However, strains extracted from the composite repair did show significant differences. Patch repairs experienced higher maximum principal strains than full-encirclement repairs with a 29.4% difference between the patch and full-encirclement repairs at 500 psi. FEA analysis also showed that maximum principal strains in the composite were insensitive to repair length past PCC-2 requirements for both repair types. This observation in the computation studies indicates that the existing extent-of-

repair (L_{over}) guidance is likely sufficient for designing patch repairs.

Pressure fatigue cycle testing was performed to compare the fatigue resistance of each repair type. Three companies from industry installed 3 patch repairs and 3 full-encirclement repairs on 6-inch OD pipes with a 0.50 in diameter circular through-wall defect. Results from the fatigue testing show that on average patch repairs lasted longer than full-encirclement repairs by 8,544 cycles. A paired t-test was performed with 95% confidence and resulted in a p-value of 0.094. This statistical testing indicates that the full-encirclement and patch repairs have statistically similar fatigue life. Fatigue testing was then performed on a large-scale specimen with a 42in OD. This test is still ongoing due to unexpected delays, but the current test results indicate that patch repairs on large diameter substrates have similar performance when compared to repairs applied on small diameter specimens.

Digital image correlation was performed to measure the full-field strains and out-of-plane displacements. Out of plane displacements found in the DIC analysis, combined with plate theory, showed that patch repairs have similar displacement profiles to full-encirclement repairs. These results also showed that both displacement profiles were below the plate theory profile. This is significant since the current design codes use plate theory to predict the interfacial fracture energy. Thus, the DIC results suggest that patch repairs may be a viable solution for repairing through-wall corrosion defects.

Based on the results in this study, patch repairs of pressure equipment are a viable option. One critical factor in the success of these types of repair is the quality of the composite installation. This factor was not directly studied in this research, but can be seen in the variability of the fatigue results on the small scale tests. Installation of repairs by appropriately

trained installers is critical to the success of all repairs, but this is especially true in the case of patch-type composite repairs.

Bibliography

[1] M. Islam, T. Aravinthan, A. Manalo, and K.-t. Lau, "Effectiveness of using fibre-reinforced polymer composites for underwater steel pipeline repairs," vol. 100, pp. 40–54, 2013.

[2] A. Mohitpour, M., Golshan, H., Murray, *Pipeline design and construction: a practical approach*. New York: ASME Press, 3rd ed., 2007.

[3] M. C. Chapetti MD, Otegaui JL, Manfredi C, "Full scale experimental analysis of stress states in sleeve repairs of gas pipelines," *International Journal of Pressure Vessels and Piping*, vol. 78, pp. 379–387, 2001.

[4] C. I. Ossai, B. Boswell, and I. J. Davies, "Pipeline failures in corrosive environments - A conceptual analysis of trends and effects," *Engineering Failure Analysis*, vol. 53, pp. 36–58, 2015.

[5] M. P. Gerhardus H. Koch, Brongers, and N. G. T. Y. P. V. J. Payer, "Corrosion costs and preventive strategies in the United States," *Summary*, pp. 1–12, 2002.

[6] J. M. Duell, J. M. Wilson, and M. R. Kessler, "International Journal of Pressure Vessels and Piping Analysis of a carbon composite overwrap pipeline repair system," *International Journal of Pressure Vessels and Piping*, vol. 85, no. 11, pp. 782–788, 2008.

[7] R. Mableson, K. R. Dunn, N. Dodds, and G. Gibson, "A NEW COMPOSITE-BASED REPAIR TECHNIQUE FOR METALLIC TUBULARS," in *FRC 2000–Composites for the Millennium*, pp. 438–445, 2000.

[8] C. Greenwood, "Composite Pipe Repair Method Shows Versatility, Long-Lasting," *Pipeline & Gas*, vol. 228, no. 2, p. 58, 2001.

[9] C. Alexander, "Development and testing of the Armor plate pipeline repair system," in *ASME energy sources technology conference*, 1999.

[10] W. K. Goertzen and M. R. Kessler, "Dynamic mechanical analysis of carbon / epoxy composites for structural pipeline repair," vol. 38, pp. 1–9, 2007.

[11] A. Baldan, "Adhesively-bonded joints and repairs in metallic alloys , polymers and composite materials : Adhesives , adhesion theories and surface pretreatment," vol. 9, pp. 1–49, 2004.

[12] W. R. True, "Composite wrap approved for U.S. gas-pipeline repairs," *Oil and Gas Journal*, vol. 93, no. 41, p. 41, 1995.

[13] D. McGeorge, A. Echtermeyer, K. Leong, B. Melve, M. Robinson, and K. Fischer, "Repair of floating offshore units using bonded fibre composite materials," *Composites Part A: Applied Science and Manufacturing*, vol. 40, pp. 1364–1380, sep 2009.

[14] DOT, "Remedial Measures: Transmission Lines," 2016.

[15] DOT, "What must I do to correct corroded pipe?," p. 195.585, 2016.

[16] ISO, "ISO 24817," 2015.

[17] ASME, "PCC-2," 2015.

[18] F. Campbell, *Manufacturing Technology for Aerospace Structural Materials*. 2006.

[19] J. Wilson, "Characterization of a carbon fiber reinforced polymer repair system for structurally deficient steel piping," 2006.

[20] J. M. Duell, J. M. Wilson, and M. R. Kessler, "International Journal of Pressure Vessels and Piping Analysis of a carbon composite overwrap pipeline repair system," *International Journal of Pressure Vessels and Piping*, vol. 85, no. 11, pp. 782–788, 2008.

[21] S. Frost, P. S. Hill, J. L. Langler, C. W. Rowley, R. H. Walker, and J. W. Wegner, "NON-METALLIC COMPOSITE REPAIR SYSTEMS FOR PIPELINES AND PIPEWORK : HIGH RISK APPLICATIONS." 2004.

[22] A. Griffith, "The Theory of Rupture," *Proceedings of the 1st Internation Conference on Applied Mechanics*.

Appendix A

FEA Material Properties

A.1 Steel Properties

Elastic Properties	
Modulus (psi)	Poisson Ratio
3.00E+07	0.3

Plasticity Curve	
Stress (psi)	Strain (in/in)
41000	0
41300	0.003395
44400	0.007734
47600	0.012213
50800	0.016268
54200	0.019878
57500	0.024347
61000	0.031909
64800	0.043747
69100	0.061653
73600	0.081793
82200	0.1695

Figure A.1: Properties for ASTM 106b steel substrate used in FEA model

A.2 Carbon Fiber Properties

Carbon Fiber Material Properties (psi)	
E1	7,130,000
E2	3,460,000
E3	3,460,000
Nu12	0.196
Nu13	0.196
Nu23	0.196
G12	88,780
G13	88,780
G23	88,780

Figure A.2: Properties for carbon fiber repair used in FEA model

Appendix B

Pipe Geometry

B.1 Small Scale

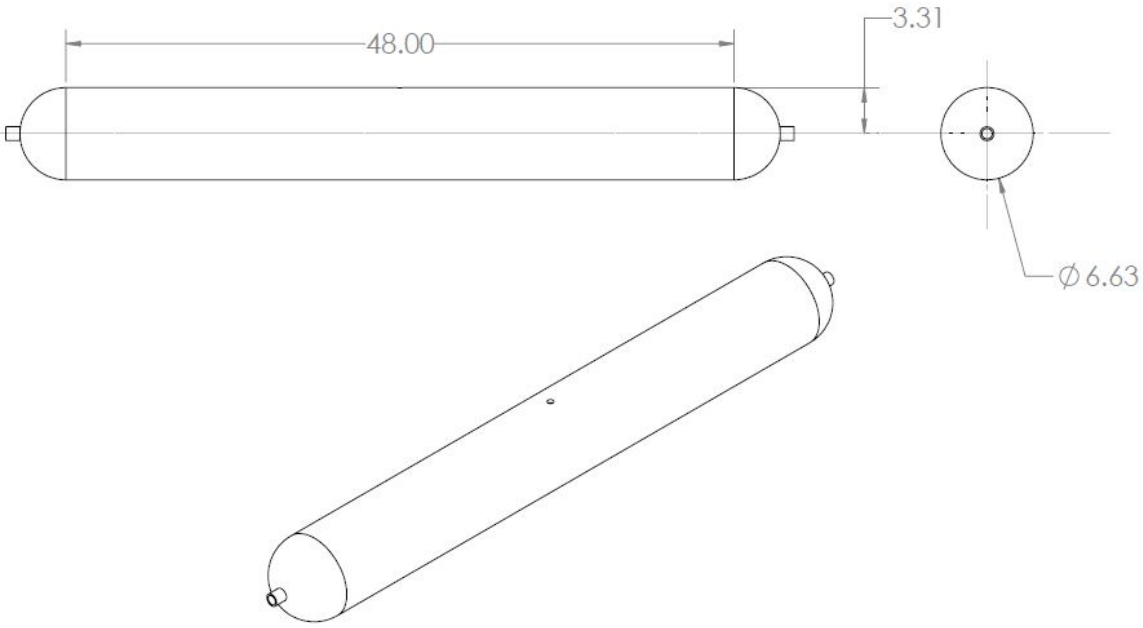

Figure B.1: Geometric dimensions for the fatigue specimens

B.2 Full Scale

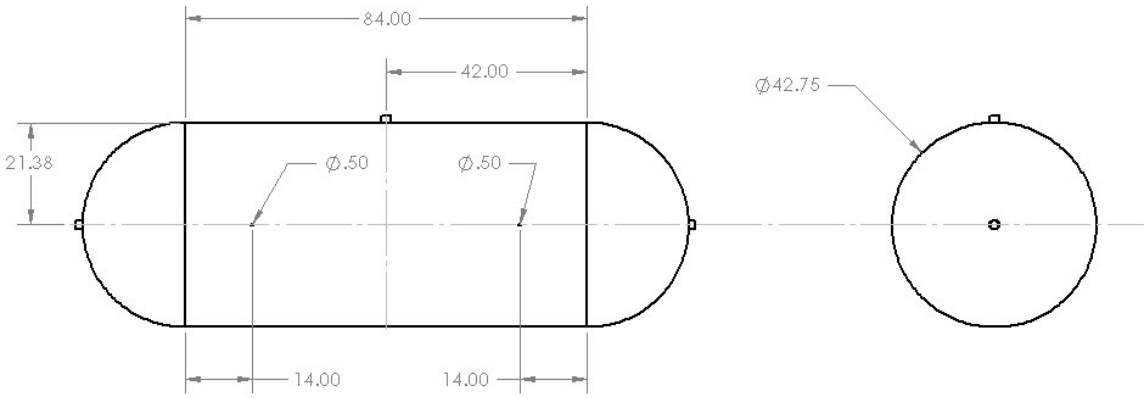

Figure B.2: Geometric dimensions for the full scale specimens

Appendix C

Wiring Diagram

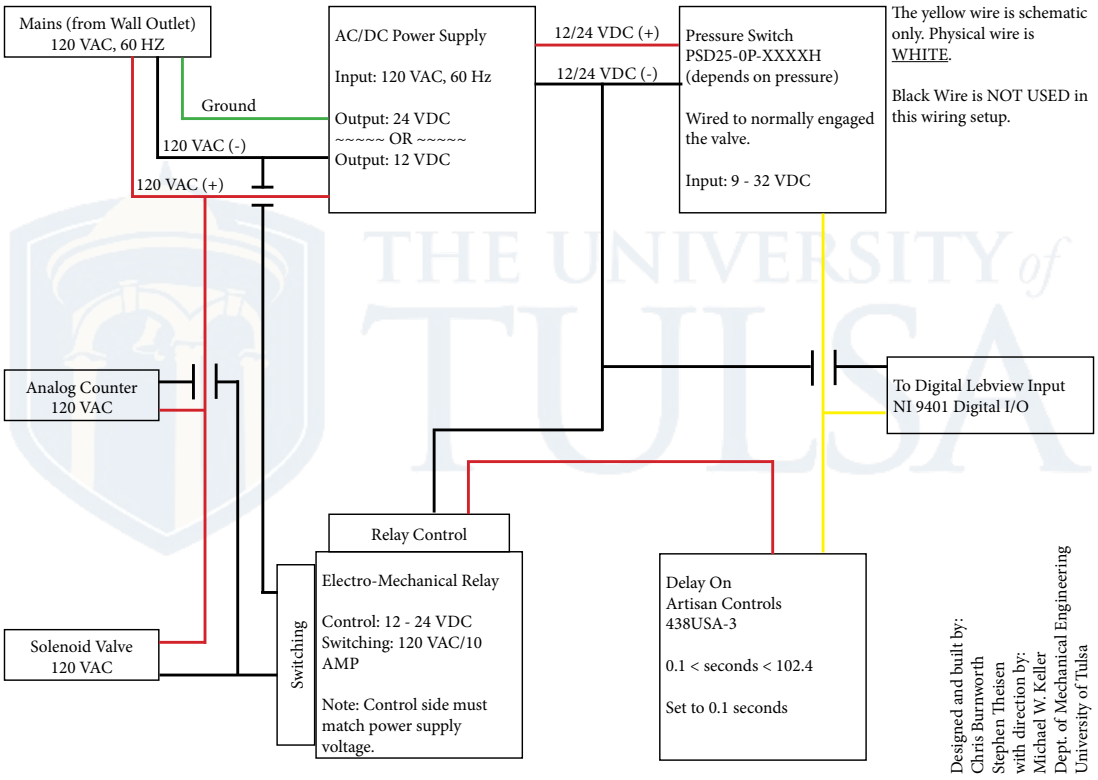

Figure C.1: Wiring diagram for the control box

Appendix D

Fatigue Summary

All fatigue test data is tabulated below along with computed t-test statistics, averages, and standard deviations. T-test statistics were calculated using a 2-tailed test with a confidence level of α = 0.05.

Company	Repair Type	Fatigue Cycles
A	Patch	9,794
	Patch	14,253
	Patch	15,231
	Full	9,942
	Full	10,051
	Full	18,976
	Average Cycles	13,041
	Standard Deviation	3,757
	P-Value	0.968
B	Patch	100,000
	Patch	100,000
	Patch	100,000
	Full	100,000
	Full	100,000
	Full	0
	Average Cycles	100,000
	Standard Deviation	0
	P-Value	N/A
C	Patch	18,284
	Patch	20,654
	Patch	40,948
	Full	314
	Full	1,254
	Full	10,278
	Average Cycles	15,289
	Standard Deviation	15,116
	P-Value	0.030

	Fatigue Life Averages	
	Patch Repair	Full Encircle Repair
A	13,093	12,990
B	100,000	100,000
C	26,629	3,949

Figure D.1: Fatigue summary for all tested specimens

Appendix E

Supplemental DIC Images

All DIC images taken are shown below to supplement those found in section 5.3. Images are sorted by company with hoop and axial strains shown for each repair type. All images were taken at design pressure of 500 psi.

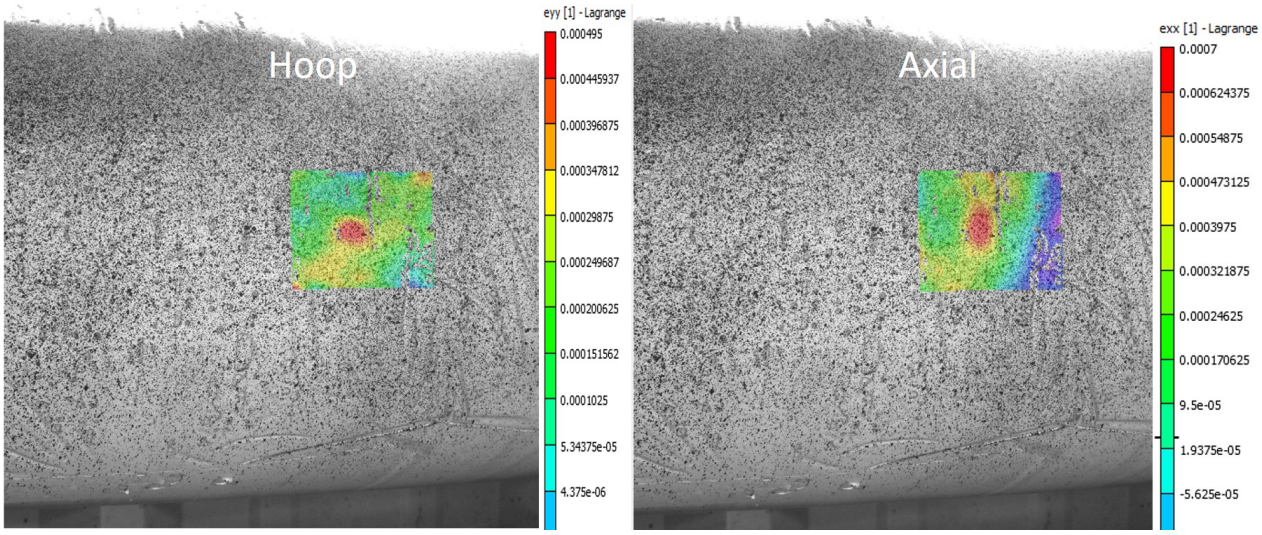

Figure E.1: Company A full encirclement DIC

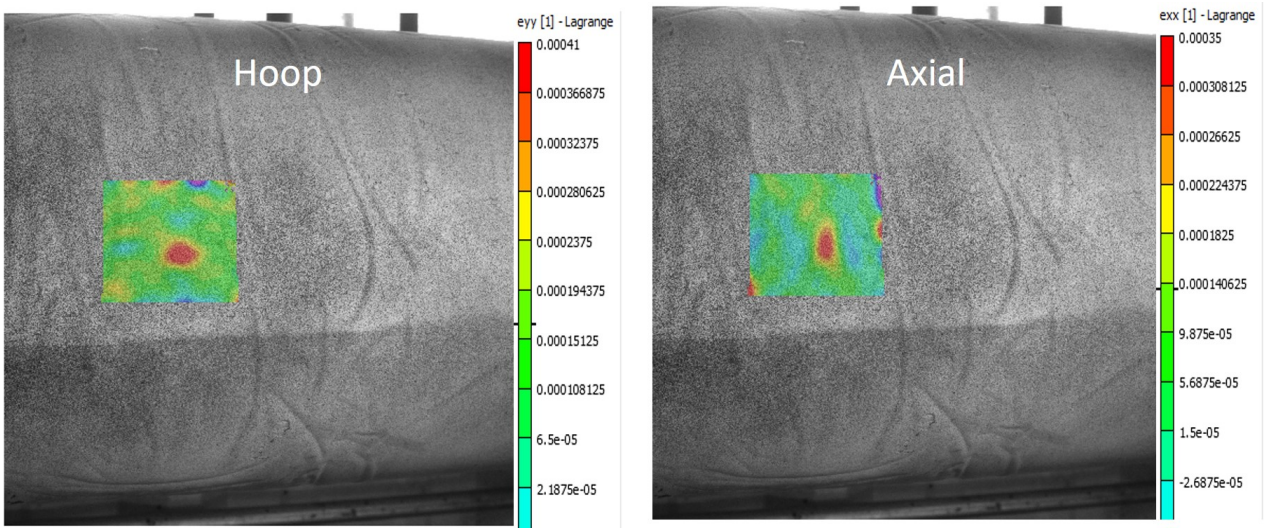

Figure E.2: Company A patch DIC

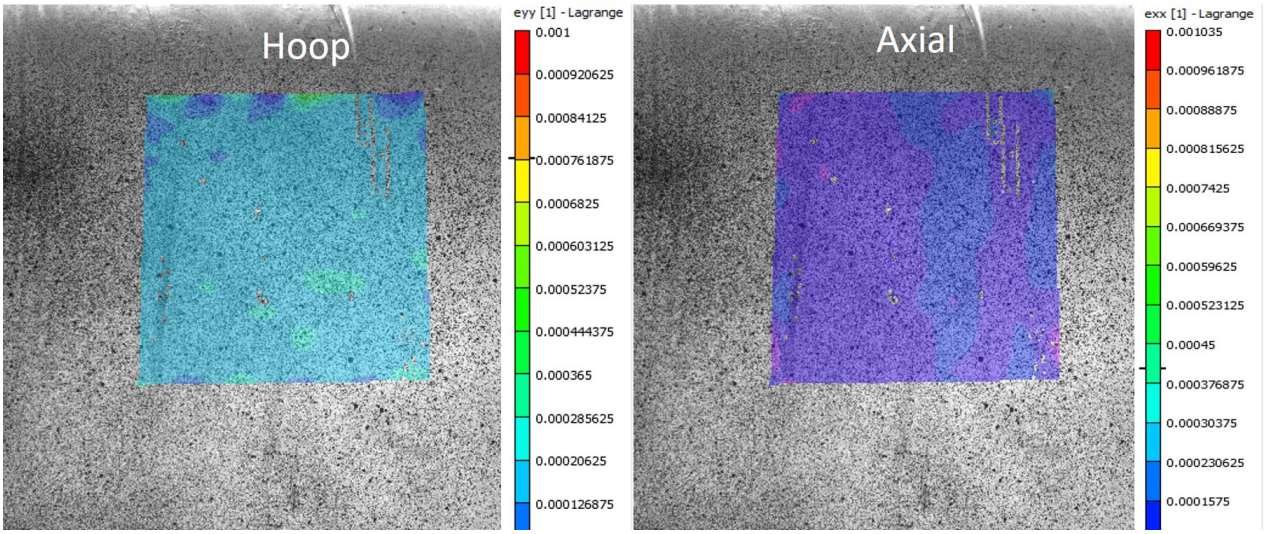

Figure E.3: Company B full encirclement DIC

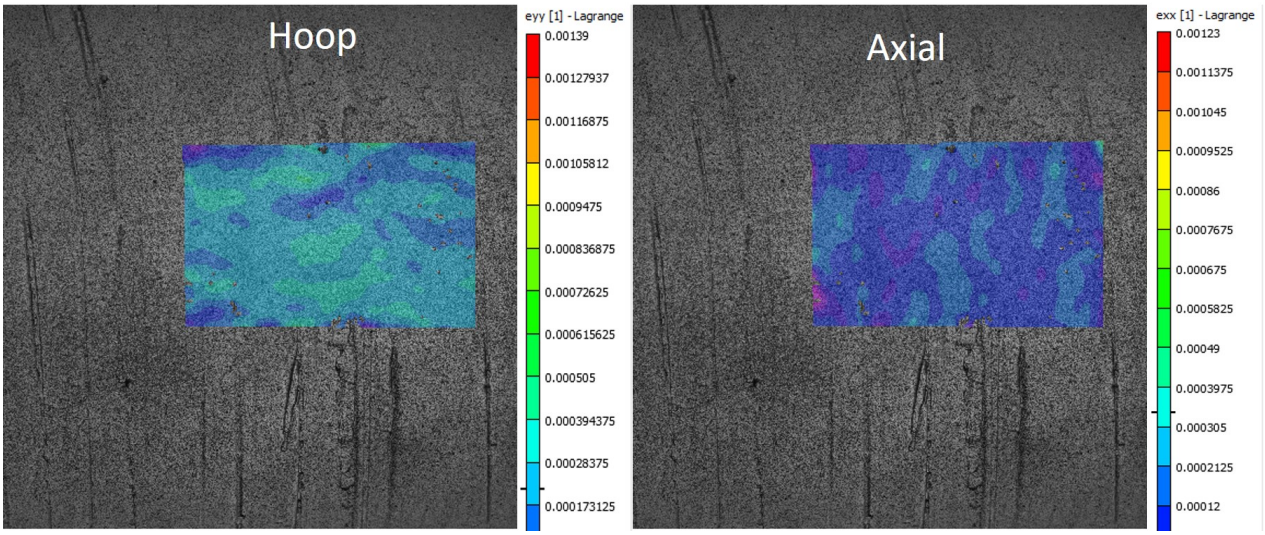

Figure E.4: Company B patch DIC

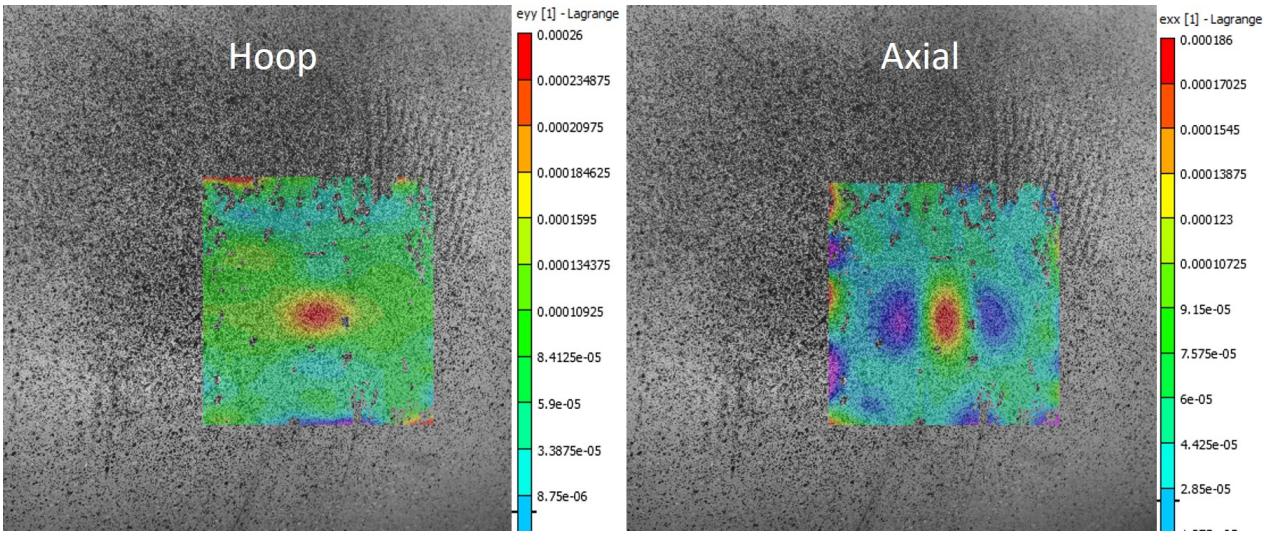

Figure E.5: Company C full encirclement DIC

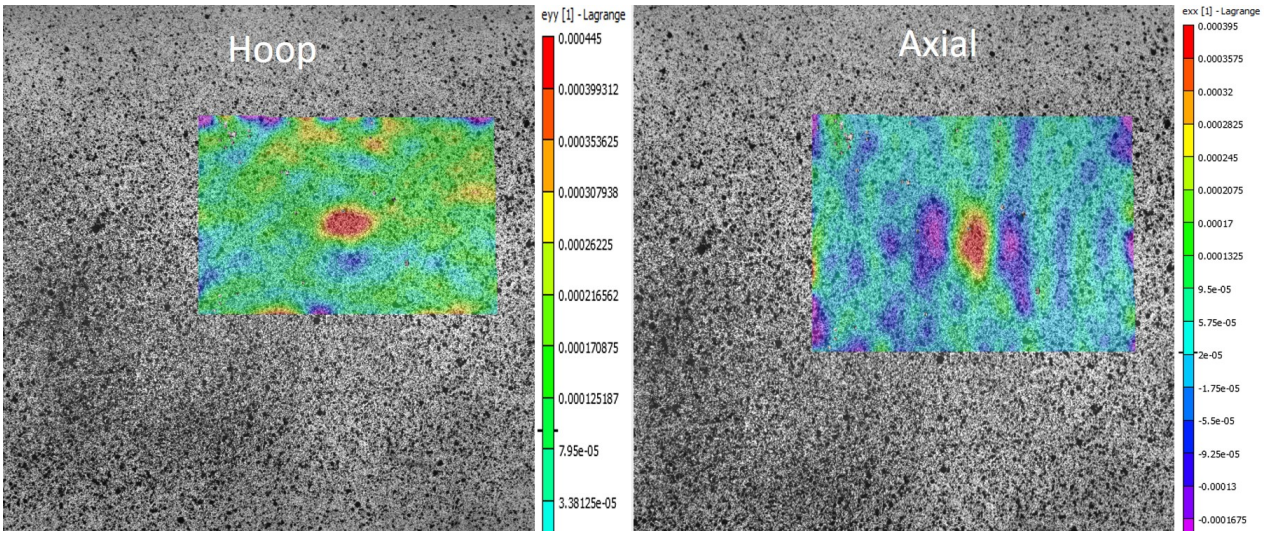

Figure E.6: Company C patch DIC